

Research Article



Natural Product Biosynthesis

How to cite: Angew. Chem. Int. Ed. 2025, 64, e202510848 doi.org/10.1002/anie.202510848

Deciphering Tryptophan Oxygenation: Key Modulators of 2-Oxindole Formation in MarE

Romie C. Nguyen, Inchul Shin,* and Aimin Liu*

Abstract: MarE, a heme-dependent aromatic oxygenase with a histidyl axial ligation, catalyzes the monooxygenation of β-methyl-L-tryptophan to form a 2-oxindole scaffold central to maremycin biosynthesis. Although structurally similar to tryptophan 2,3-dioxygenase (TDO), which initiates L-tryptophan catabolism via dioxygenation, MarE exhibits distinct reactivity modulated by ascorbate. While ascorbate has no effect on TDO, it promotes selective monooxygenation by MarE. In its absence, MarE favors dioxygenation and formation of pyrroloindoline products, revealing latent catalytic versatility. Active-site loop sequences differ between the two enzymes, SLGGR in MarE versus GTGGS in TDO, prompting loop-swapping experiments to probe structure-function relationships. Substituting GTGGS in TDO to MarE-like sequences (GTGGA or SLGGS) shifted reactivity toward monooxygenation and formation of C3-hydroxylated, non-oxindole products that underwent further cyclization into tricyclic structures. Conversely, replacing SLGGR in MarE with GTGGS resulted in enhanced C2,C3-dioxygenation nearly 4-fold. These results underscore the active-site loop as a key determinant of oxidation outcome, alongside the modulatory role of ascorbate. By revealing the true catalytic identity of MarE and delineating the roles of small-molecule effectors and loop architecture, this study advances mechanistic understanding and predictive capabilities within the oxygenase superfamily.

The aromatic amino acid tryptophan plays a wide variety of roles in nature and serves as an important precursor for synthesizing proteins, neurotransmitters, their regulators, redox carriers, and natural products. Tryptophan dioxygenases, such as indoleamine 2,3-dioxygenase (IDO) and tryptophan 2,3-dioxygenase (TDO), catalyze the heme-dependent insertion of molecular oxygen into the indole ring of their substrate, L-tryptophan (L-Trp, 2) producing N-formylkynurenine (NFK, 2d), without the need for additional electrons and protons (Scheme 1a). [1-2]

Recent bioinformatic analyses and structural alignments have revealed that these tryptophan dioxygenase enzymes are part of a larger protein group known as the histidyl-ligated heme-dependent aromatic oxygenase

[*] R. C. Nguyen, Prof. Dr. I. Shin, Prof. Dr. A. Liu Department of Chemistry, The University of Texas at San Antonio, Texas, U.S.A.

E-mail: Inchul.Shin@utsa.edu Feradical@utsa.edu

Abbreviations: β -Me-L-Trp, (25,35)- β -methyl-L-tryptophan; HDAO, heme-dependent aromatic oxygenase; IDO, indoleamine 2,3-dioxygenase; TDO, tryptophan 2,3-dioxygenase; IPA, indole-3-propionic acid; L-Trp, L-tryptophan; NFK, *N*-formylkynurenine; TyrH, tyrosine hydroxylase..

- Additional supporting information can be found online in the Supporting Information section
- © 2025 The Author(s). Angewandte Chemie International Edition published by Wiley-VCH GmbH. This is an open access article under the terms of the Creative Commons Attribution License, which permits use, distribution and reproduction in any medium, provided the original work is properly cited.

(HDAO) superfamily.^[3] This structure-based, functionally related superfamily includes thousands of members with subgroups that oxidize tryptophan or tyrosine and their metabolites. Some, like IDO/TDO, initiate tryptophan catabolism and serve as immune checkpoints, exploited by cancers for immune evasion.^[4–5] Others, such as MarE, SfmD, and TyrH, are critical in building the core structure of bioactive natural products from amino acids in secondary metabolism.^[6–10] Thus, the functions of HDAO members exhibit substantial implications across multiple scientific domains.

MarE is a recently identified enzyme that, in the presence of ascorbate, catalyzes the monooxygenation of (2S,3S)- β -methyl-L-tryptophan $(\beta$ -Me-L-Trp, 1) to produce a unique 2-oxindole (1a) product (Scheme 1b). [6] The crystal structure of this enzyme firmly assigns MarE as a member of the HDAO superfamily. [11] The 2-oxindole moiety serves as a key scaffold for the synthesis of a variety of bioactive compounds, [6,12] such as maremycins (Scheme 1c), which exhibit antimicrobial activity, and spirooxindoles, which serve as a promising scaffold for anticancer agents (Scheme 1d). [6,13–14]

In the enzyme-substrate complex crystal structure, β -Me-L-Trp binds to the distal heme pocket of MarE analogous to how L-Trp binds in the active site of IDO/TDO. [11] Both enzymes share similar protein structure and substrate interaction modes. However, the structural advancements do not address the intriguing reaction outcomes of these enzymes. Specifically, it remains unclear why MarE functions as a monooxygenase enzyme that catalyzes a single C2 oxygenation, [6.11] whereas IDO/TDO produces a C2,C3-dioxygenated product (2d) through a stepwise O-atom transfer reaction process, [15-18] which is a common conundrum in these enzymes and synthetic model complexes. [19-22]

15213773, 2025, 35, Downloaded from https://onlinelibrary.wiley.com/doi/10.1002/anie.202510848 by University Of Texas At San Antonio Libraries, Wiley Online Library on [01/09/2025]. See the Terms

on Wiley Online Library for rules of use; OA articles are governed by the applicable Creative Commons License

Scheme 1. Reactions catalyzed by IDO/TDO a) and MarE b). Naturally occurring maremycins A, B, C1, C2, D1, D2, E, and F c) and spirooxindoles d) share an oxindole structure (maroon color).

To tackle this enigma, we conducted a detailed analysis of the MarE-catalyzed reaction to elucidate the governing factors for its preference for 2-oxindole formation. In the O_2 -dependent monooxygenation, β -Me-L-Trp provides $2e^-$ to O_2 . The overall reaction requires an additional $2e^-$ and $2H^+$ to reduce O_2 , suggesting an external electron donor, i.e., a cosubstrate, is missing from the reaction of MarE. We then conducted the reaction with and without an additional reducing agent to determine its role in the process. This approach aims to provide a comprehensive understanding of the reaction components.

We observed five reaction products using a full-spectrum HPLC detector when examining the wild-type ferrous heme-containing MarE reaction profile with ${\bf 1}$ in oxygen-saturated buffer and without any cosubstrate (Figure 1a). The product ${\bf 1a}$ was a monooxygenated result with all the characteristics identical to the previously reported 2-oxindole product. Surprisingly, the primary reaction product (${\bf 1b}$) and a minor product ${\bf 1b}_1$ were dioxygenated products, each exhibiting a 32-Da increase from ${\bf 1}$ (Figure 1b).

The chemical structures of those newly identified MarE reaction products were determined by NMR (Figure 2). Product 1b is a mixture of stereoisomers of the NFK-like pyrrole ring-opened dioxygenated products at 1:1.3 ratio (Figure S1 and Table S2). Product 1b1 is a dioxygenated product containing a 2-oxindole ketone moiety and an additional hydroxylation at C3 (Figure S2 and Table S3). Products 1a₁ and 1a2 are diastereomers containing a C3-monooxygenated tricyclic pyrroloindoline structure similar to the previously identified TDO C3-monooxygenated furoindoline product, utilizing a substrate analog of 2 that substitutes the α amino nitrogen with oxygen (Figure \$3 and Table \$4).[18] The structure of $1a_1$ appears to be an isomer of $1a_2$, with the chemical shift of its C2 proton appearing slightly more upfield compared to 1a₂ (Figure S4 and Table S5). Together, these results reveal the true colors of MarE's catalytic versatility, producing monooxygenated, dioxygenated, and pyrroloindoline products.

Based on these results, an additional factor outside the enzyme must be present to drive the reaction toward monooxygenation. We revisited common electron donors, and our results indicated that the monooxygenated 2-oxindole

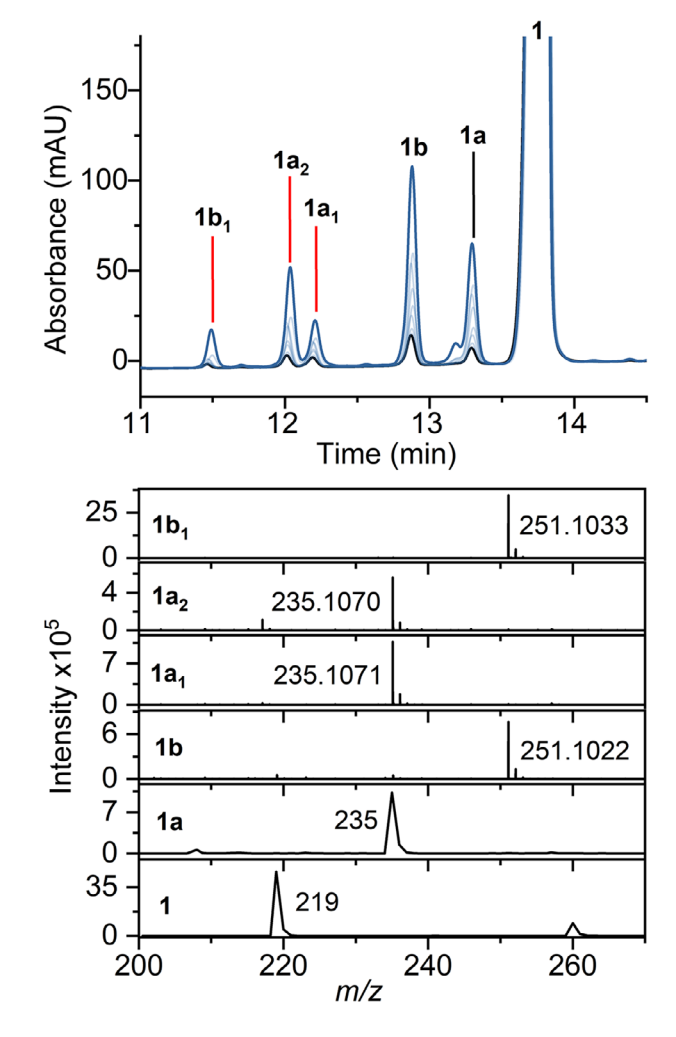


Figure 1. MarE reaction with β -Me-L-Trp (1) and O₂. Top panel HPLC time course (10 min: black, 16 h: blue). Bottom panel HRMS analysis. Products: 1a (2-oxindoline product), 1a₁, and 1a₂ (monooxygenated products), 1b and 1b₁ (dioxygenated products).

product **1a** was predominantly produced from **1** in the presence of ascorbate (Figure 3, inset), echoing the previous study. However, unlike the previous report, we detected a minor dioxygenated product **1b** exhibiting the characteristic

15213773, 2025, 35, Downloaded from https://onlinelibrary.wiley.com/ob/10.1002/anie.202510848 by University Of Texas At San Antonio Libraries, Wiley Online Library on [01/09/2025]. See the Terms

on Wiley Online Library for rules of use; OA articles are governed by the applicable Creative Commons License

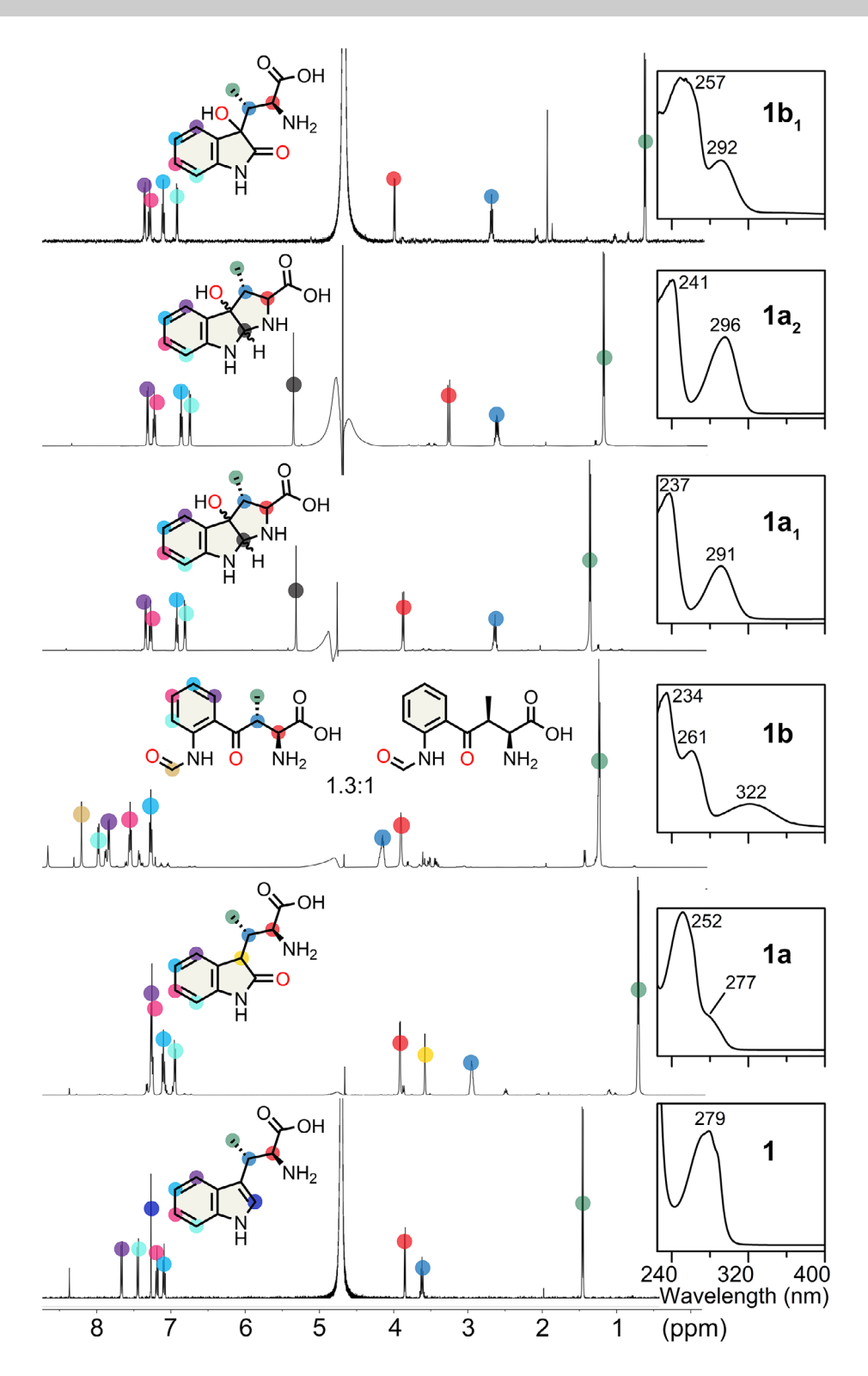


Figure 2. MarE reaction without ascorbate: 2-oxindole, dioxygenation, and pyrroloindoline products of β-Me-L-Trp (1) characterized by ¹H-NMR and UV–vis spectroscopies.

UV-vis spectral feature of NFK at 322 nm and a 32 Da mass increase (Figure S5). A second minor monooxygenated product 1c eluted the earliest, sharing similar UV-vis spectral features and m/z of 235 (Figure S6) with 1a in a much-reduced quantity (Figure S5). These results suggest that an

electron donor such as ascorbate is a critical factor in driving MarE toward monooxygenation but remains insufficient to function as the sole factor responsible for single oxygen insertion, specifically at the C2 position. The product distribution shift observed with ascorbate raises questions about

15213773, 2025, 35, Downloaded from https://onlinelibrary.wiley.com/doi/10.1002/anie.202510848 by University Of Texas At San Antonio Libraries, Wiley Online Library on [01/09/2025]. See the Terms

and-conditions) on Wiley Online Library for rules of use; OA articles are governed by the applicable Creative Commons License

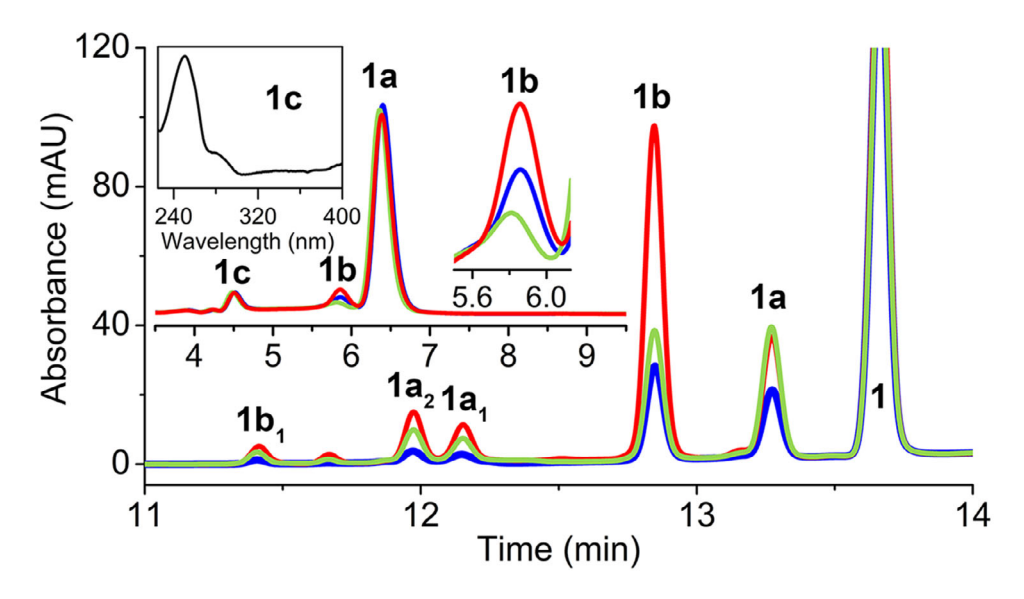


Figure 3. Reaction of 1 in the absence of ascorbate with wild-type MarE (blue), SLGGR-to-SLGGS (light green), and <u>SLGGR-to-GTGGS</u> (red) MarE variants. The insets show the reaction of MarE and its variants in the presence of ascorbate and include the zoomed-in view for peak 1b and UV-vis spectrum of 1c.

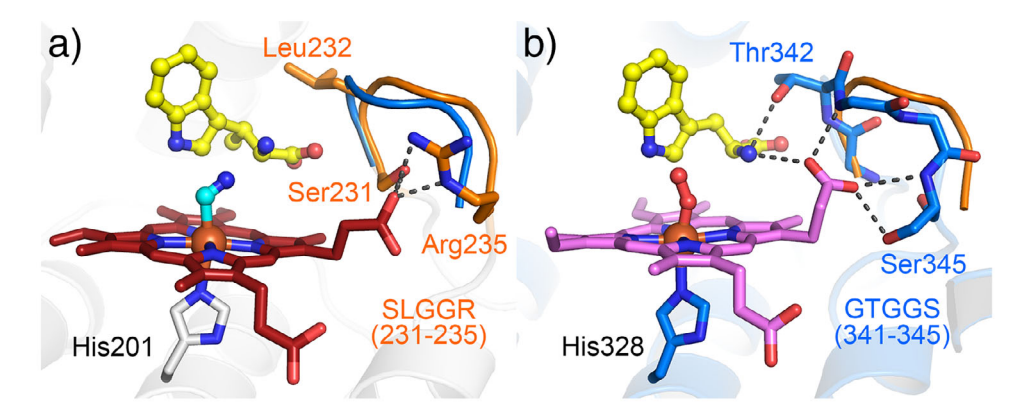


Figure 4. Second coordination sphere comparison. a) MarE (orange, SLGGR loop with β-Me-L-Trp in yellow, 9CA3.pdb) versus b) TDO (blue, GTGGS loop with L-Trp/O₂, 5TI9.pdb). The substrates are shown with their carbons in yellow. The GTGGS loop of TDO (blue) is overlaid with SLGGR loop of MarE (orange).

its physiological relevance. Notably, *Streptomyces sp.* B9173 (also known as *S. rishiriensis*), the native producer of MarE, encodes a homolog of rat L-gulonolactone oxidase—the terminal enzyme in the biosynthetic pathway converting L-gulono- γ -lactone to ascorbate. This implies that the organism may endogenously generate ascorbate or a similar reductant. Importantly, in the absence of ascorbate, MarE yields a broader set of oxygenated products, many lacking the 2-oxindole moiety observed under reducing conditions. Thus, ascorbate not only modulates product selectivity but may also reflect a native cofactor environment relevant to MarE's physiological function.

Next, we explored additional factors influencing reaction outcomes. Structural comparison between MarE with IDO and TDO revealed that the SLGGR loop of MarE (residues 231 to 235) corresponds to the conserved GTGGS sequences in IDO/TDO in the catalytic active site (Figures 4a and S7). The GTGGS (residues 341 to 345 in human TDO numbering)

is part of the large JK-loop,^[1] which bridges the substrate amino group to the heme propionate positioned above the heme plane (hereafter, the up-propionate) (Figure 4b). Notably, the GTGGS loop forms an H-bond with the α -amino nitrogen of L-Trp (Figure 4b),^[23–25] suggesting a catalytic role for this loop in IDO and TDO, though its precise impact on the reaction remains unclear.

We then experimentally examined how loop differences influence catalysis in MarE and human TDO. A single-point mutation in the right end of the TDO loop (GTGGS-to-GTGGA) enhanced monooxygenation when using indole-3-propionic acid (IPA, 3), a mechanistic probe lacking the α -amino group of L-Trp (Figure S8). Compared to wild-type TDO, this variant produced \sim 1.4-fold more monooxygenated 2-oxindole product 3b (Figure S8 and Scheme 2). However, when tested with L-Trp (2), the single-point mutation had no discernible impact, yielding a product distribution nearly identical to wild-type TDO (Figure S9).

15213773, 2025, 35, Downloaded from https://onlinelibrary.wiley.com/doi/10.1002/anic.202510848 by University Of Texas At San Antonio Libraries, Wiley Online Library on [01/09/2025]. See the Terms and Conditions (https://onlinelibrary.wiley.com/

and-conditions) on Wiley Online Library for rules of use; OA articles are governed by the applicable Creative Commons License

Scheme 2. Oxygenation products of the MarE-mediated oxidation reactions identified in this study (m/z values in parentheses).

We then tested Thr342, which is H-bonded to the substrate. A double mutation (GTGGS-to-SLGGS) at the loop's front end reduced dioxygenation efficiency toward L-Trp. The reaction of this variant primarily yielded 2d, the expected NFK product (\sim 95%), but also generated a minor $(\sim 5\%)$ monooxygenated product **2e** distinct from the 2oxindole observed in MarE (Figure 5 and Figure \$10). The UV-vis spectrum of this minor product 2e aligns well with 1a₁, 1a₂, and 4, consistent with previous TDO reactions using an N-to-O substituted L-Trp analog (Figure 5 inset), whose chemical structure has been fully elucidated by HRMS and NMR.[18] Thus, 2e underwent hydroxylation at C3, triggering spontaneous cyclization into a tricyclic structure as previously found for 4. Using the native substrate of MarE (1), this TDO variant produced three products: a monooxygenated species 1e, though not a 2-oxindole, and two NFK-like dioxygenated products, 1d and 1d' (Figure S11 and

Challenging MarE with the non-native substrate L-Trp (2) resulted in cross-reactivity and complex product distribution (Figure S12A). Two monooxygenated products, **2a** and **2a'** exhibited UV-vis spectral features similar to the 2-oxindole-containing product **1a** (Figure 2 and S12B), and their identical m/z values (221) confirmed them as 2-oxindole derivatives of **2** (Figure S12C and Scheme 2). However, the <u>SL</u>GGR-to-GTGGR MarE variant showed no significant change in the distribution of mono- and dioxygenated products compared

to wild-type MarE (Figures S12A and S5A), indicating that the SLGGR loop composition in MarE has a less pronounced impact than its counterpart in TDO. Structural analysis further supported this, as the α -amino group of 1 does not interact with this loop (Figure 4a).

The reciprocal SLGGR-to-GTGGS loop swap triple mutation in MarE, which fully mimics the TDO loop, increased C3 oxygenation in the presence of ascorbate, lead to a 1.6-fold increase in the C2,C3-dioxygenated product 1b (Figure 3). The reaction of this mutant in the absence of ascorbate resulted in a near 4-fold increase of dioxygenated product 1b. This substantial shift underscores the critical role of the loop region in promoting dioxygenation chemistry and highlights that the observed effect is not solely attributable to ascorbate but rather to the structural mimicry of the TDO active site loop. This loop likely plays a direct role in controlling substrate positioning and O2 access, thereby influencing whether a mono- or dioxygenation event occurs. When this loop is mutated to mimic the GTGGS motif found in TDO, the production of the NFKlike dioxygenation product markedly increases—even in the absence of ascorbate—supporting the idea that loop dynamics and structural geometry are central to oxygenation outcomes. These loop studies illustrate that this region plays a crucial role in directing mono- versus dioxygenation chemistry, with its influence being substrate-dependent (i.e., influenced by the presence or absence of the α -amino group),

15213773, 2025, 35, Downloaded from https://onlinelibrary.wiley

.com/doi/10.1002/anie.202510848 by University Of Texas At San Antonio Libraries, Wiley Online Library on [01/09/2025]. See the Terms and Conditions (https://onlinelibrary.wiley.

and-conditions) on Wiley Online Library for rules of use; OA articles are governed by the applicable Creative Commons License

Figure 5. Monooxygenation by GTGGS-to-SLGGS TDO variant. HPLC chromatogram: wild-type (blue) and variant (red). Product 2e (red) UV-vis versus 4 (black). Structures of 2e and 4 are shown.

enzyme-context-dependent due to variations in loop composition, and ascorbate dependent.

To further evaluate structural contributions to oxygenation outcomes and enhance scientific rigor, we examined differences in other regions including near the heme propionate below the plane (the down-propionate) (Figure S13). In TDO, Arg159 and Tyr350 directly interact with the down-propionate, while Arg325, positioned 3.5 Å away, may contribute indirectly to the heme environment, either through electrostatic interactions with the heme propionate or via bridging water molecules. Such distal interactions are commonly observed in heme enzymes and are known to influence heme orientation, redox properties, and reactivity. In contrast, MarE's down-propionate interacts solely with Arg243.

R159A, Y350F, and R325A mutants in TDO were generated. When challenged with L-Trp (2), these mutations had minimal impact, as all variants produced similar amounts of NFK (2d) as the wild-type enzyme (Figure S14). However, with IPA (3), these TDO mutants exhibited increased monooxygenation. Compared to wild-type TDO, Y350F, R159A, and R325A produced approximately 3.8-, 3.7-, and 1.5-fold more of the monooxygenated product 3b, respectively (Figure \$15). In contrast, the TDO loop variants, except the single-point mutation, did not enhance the 3b formation (Figure S8). These indicate that the down-propionate region in TDO plays a role in substrate selectivity and product outcome, particularly when the substrate lacks an α -amino group, as previously expected for another HDAO enzyme TvrH.[26] All generated TDO variants exhibited reduced production of dioxygenated product 3c relative to wild-type enzyme (Figures S8, S15, and S17). Similarly, MarE loop variants produced more 3b and less 3c than wild-type MarE (Figures S15–S17), suggesting that the TDO-mimicking loop in MarE has little influence when the substrate lacks an α amino group. These variant studies indicate that modifications in the down-propionate region led to shifts in reactivity with IPA (3) versus β -Me-L-Trp (1), suggesting that the region may indirectly affect substrate orientation or accessibility of reactive oxygen species, thereby contributing to substrate discrimination. While not a part of the substrate binding pocket per se, this region appears to act as a functional gatekeeper, tuning the enzyme's reactivity landscape in a substrate-dependent manner.

This work reveals a more nuanced view of MarE's reactivity, showing that it is not strictly a monooxygenase—as previously assumed—but functions primarily as a dioxygenase. Ascorbate emerges as the primary determinant of monooxygenation in this experimental system. The shift in product profile in the presence of ascorbate suggests that redox conditions can modulate the enzyme's catalytic pathway, but only within the structural context of MarE. This modulation likely depends on features such as the flexible SLGGR loop adjacent to the active site. Moreover, the identification of a novel three-ring monooxygenated product connects MarE's activity to natural product biosynthesis in Streptomyces sp. B9173. Given the precedent for similar scaffolds in other Streptomyces-derived metabolites, this enzyme may serve as a biosynthetic entry point to a broader array of structurally diverse compounds.

Our data supports a mechanistic model in which MarE's oxygenation profile is dictated by a combination of loop-dependent substrate control and ascorbate-modulated redox flexibility—features not shared by IDO/TDO and other known HDAO enzymes involved in metabolizing tryptophan and its derivatives. Ascorbate emerges as the primary determinant of monooxygenation in this experimental system, while active-site features—such as the SLGGR loop in MarE and the GTGGS loop in IDO/TDO—fine-tune oxidation site selectivity. In the presence of ascorbate, MarE predominantly enforces preferential C2 monooxygenation of β -Me-L-Trp (1), whereas IDO/TDO are guided by their

Research Article



15213773, 2025, 35, Downloaded from https://onlinelibrary.wiley.com/doi/10.1002/anie.202510848 by University Of Texas At San Antonio Libraries, Wiley Online Library on [01/09/2025]. See the Terms

onditions) on Wiley Online Library for rules of

are governed by the applicable Creative Commons License

distinct loop architecture and facilitates sequential C3 and C2 dioxygenation of L-Trp (2). The structure-function relationship described here highlights broader implications for heme-enzyme-mediated aromatic amino acid oxidations in metabolism and natural product biosynthesis.

Supporting Information

Materials and Methods, (Tables S1–S5), (Figures S1–S17), and associated references.

Acknowledgements

The authors deeply appreciate that Dr. Frances Arnold provided the expression vector of PfTrpB^{2B9} to synthesize β -Me-L-Trp. The authors thank Dr. Wendell P. Griffith at UTSA Mass Spectrometry & Proteomics Core Facility for obtaining HRMS data, and the authors appreciate the productive discussion with Dr. Daniel Wherritt regarding NMR structural identifications. The authors thank Samuel R. Montoya for initial contributions to this work. This work was supported by NIH grant GM108988, Welch Foundation grants AX-2110–20220331 and AX-2110–20250403, and the Lutcher Brown Distinguished Chair endowment.

Conflict of Interests

The authors declare no conflict of interest.

Data Availability Statement

The data that support the findings of this study are available in the Supporting Information of this article.

Keywords: Dioxygenase • Enzyme Mechanism • Monooxygenase • Natural product biosynthesis • Oxindole

- [1] Z. Geeraerts, I. Ishigami, Y. Gao, S. R. Yeh, J. Inorg. Biochem. 2024, 261, 112707.
- [2] E. S. Millett, I. Efimov, J. Basran, S. Handa, C. G. Mowat, E. L. Raven, Curr. Opin. Chem. Biol. 2012, 16, 60–66.
- [3] I. Shin, Y. Wang, A. Liu, Proc. Natl. Acad. Sci. USA 2021, 118, e2106561118.
- [4] I. Cervenka, L. Z. Agudelo, J. L. Ruas, Science 2017, 357, eaaf9794.
- [5] N. J. Cundy, R. K. Hare, T. Tang, A. G. Leach, T. A. Jowitt, O. Qureshi, J. Gordon, N. M. Barnes, C. A. Brady, E. L. Raven,

- R. S. Grainger, S. Butterworth, *RSC Chem. Biol.* **2021**, 2, 1651–1660.
- [6] Y. Zhang, Y. Zou, N. L. Brock, T. Huang, Y. Lan, X. Wang, Z. Deng, Y. Tang, S. Lin, J. Am. Chem. Soc. 2017, 139, 11887–11894.
- [7] I. Shin, I. Davis, K. Nieves-Merced, Y. Wang, S. McHardy, A. Liu, Chem. Sci. 2021, 12, 3984–3998.
- [8] Y. Wang, I. Davis, I. Shin, H. Xu, A. Liu, J. Am. Chem. Soc. 2021, 143, 4680–4693.
- [9] Y. Wang, I. Davis, I. Shin, D. J. Wherritt, W. P. Griffith, K. Dornevil, K. L. Colabroy, A. Liu, ACS Catal. 2019, 9, 4764–4776.
- [10] X. Shi, G. Zhao, H. Li, Z. Zhao, W. Li, M. Wu, Y. L. Du, Nat. Chem. Biol. 2023, 19, 1415–1422.
- [11] I. Shin, R. C. Nguyen, S. R. Montoya, A. Liu, J. Biol. Chem. 2025, 301, 108241.
- [12] Y. M. Khetmalis, M. Shivani, S. Murugesan, K. V. G. Chandra Sekhar, *Biomed. Pharmacother.* 2021, 141, 111842.
- [13] Y. Zou, Q. Fang, H. Yin, Z. Liang, D. Kong, L. Bai, Z. Deng, S. Lin, Angew. Chem. Int. Ed. 2013, 52, 12951–12955.
- [14] B. Yu, D.-Q. Yu, H.-M. Liu, Eur. J. Med. Chem. 2015, 97, 673–
- [15] A. Lewis-Ballester, D. Batabyal, T. Egawa, C. Lu, Y. Lin, M. A. Marti, L. Capece, D. A. Estrin, S. R. Yeh, *Proc. Natl. Acad. Sci. USA* 2009, 106, 17371–17376.
- [16] L. W. Chung, X. Li, H. Sugimoto, Y. Shiro, K. Morokuma, J. Am. Chem. Soc. 2010, 132, 11993–12005.
- [17] J. Basran, I. Efimov, N. Chauhan, S. J. Thackray, J. L. Krupa, G. Eaton, G. A. Griffith, C. G. Mowat, S. Handa, E. L. Raven, J. Am. Chem. Soc. 2011, 133, 16251–16257.
- [18] I. Shin, B. R. Ambler, D. Wherritt, W. P. Griffith, A. C. Maldonado, R. A. Altman, A. Liu, J. Am. Chem. Soc. 2018, 140, 4372–4379.
- [19] G. B. Tolbert, S. B. Jayawardana, Y. Lee, J. Sun, F. Qu, L. M. Whitt, H. S. Shafaat, G. B. Wijeratne, *Chemistry* **2024**, *30*, e202402310
- [20] P. Mondal, S. Rajapakse, G. B. Wijeratne, J. Am. Chem. Soc. 2022, 144, 3843–3854.
- [21] M. Mukherjee, A. Dey, JACS Au 2021, 1, 1296-1311.
- [22] P. Mondal, G. B. Wijeratne, J. Am. Chem. Soc. 2020, 142, 1846– 1856
- [23] F. Forouhar, J. L. Anderson, C. G. Mowat, S. M. Vorobiev, A. Hussain, M. Abashidze, C. Bruckmann, S. J. Thackray, J. Seetharaman, T. Tucker, R. Xiao, L. C. Ma, L. Zhao, T. B. Acton, G. T. Montelione, S. K. Chapman, L. Tong, *Proc. Natl. Acad. Sci.* USA 2007, 104, 473–478.
- [24] A. Lewis-Ballester, F. Forouhar, S. M. Kim, S. Lew, Y. Wang, S. Karkashon, J. Seetharaman, D. Batabyal, B. Y. Chiang, M. Hussain, M. A. Correia, S. R. Yeh, L. Tong, *Sci. Rep.* 2016, 6, 35169
- [25] A. Lewis-Ballester, K. N. Pham, D. Batabyal, S. Karkashon, J. B. Bonanno, T. L. Poulos, S. R. Yeh, *Nat. Commun.* 2017, 8, 1693.
- [26] W. Peng, S. Yan, X. Zhang, L. Liao, J. Zhang, S. Shaik, B. Wang, J. Am. Chem. Soc. 2022, 144, 20484–20494.

Manuscript received: May 18, 2025 Accepted manuscript online: June 24, 2025 Version of record online: July 20, 2025

Supporting Information

Deciphering Tryptophan Oxygenation: Key Modulators of 2-Oxindole Formation in MarE

Romie C. Nguyen, Inchul Shin*, and Aimin Liu*

Department of Chemistry, The University of Texas at San Antonio, Texas 78249, United States

*To whom correspondence should be addressed:

Aimin Liu (e-Mail: Feradical@utsa.edu) or Inchul Shin (e-Mail: Inchul.Shin@utsa.edu)

DOI: 10.1002/anie.202510848 SI 1 of 28

Materials and Methods

β-Me-L-Trp preparation

Cloning, expression, and purification of MarE

Heme reconstitution of MarE

Pyridine hemochromagen assay

Enzyme reaction

High-performance liquid chromatography coupled with mass spectrometry (LC-MS)

High resolution mass spectrometry (HRMS)

Scaled-up enzyme reaction and product purification for NMR

List of Supplementary Tables

Table S1	The codon-optimized DNA sequence of MarE and primers used in this study for MarE and
	human TDO mutagenesis studies
Table S2	1 H-NMR (500 MHz, D $_{2}$ O) and 13 C-NMR (126 MHz, D $_{2}$ O) for MarE product 1b
Table S3	1 H-NMR (500 MHz, D $_{2}$ O) and 13 C-NMR (126 MHz, D $_{2}$ O) for MarE product ${f 1b_{1}}$
Table S4	1 H-NMR (500 MHz, D $_{2}$ O) and 13 C-NMR (126 MHz, D $_{2}$ O) for MarE product 1a$_{2}$
Table S5	1 H-NMR (500 MHz, D $_{2}$ O) and 13 C-NMR (126 MHz, D $_{2}$ O) for MarE product ${f 1a_{1}}$

List of Supplementary Figures

Figure S1	1 H- and 13 C-NMR of product ${f 1b}$ in D $_{2}$ O from the MarE reaction with dioxygen
Figure S2	1 H- and 13 C-NMR of product ${f 1b_1}$ in ${f D_2O}$ from the MarE reaction with dioxygen
Figure S3	1 H- and 13 C-NMR of product 1a₂ in D ₂ O from the MarE reaction with dioxygen
Figure S4	1 H- and 13 C-NMR of product $\mathbf{1a_{1}}$ in D_{2} O from the MarE reaction with dioxygen
Figure S5	Reaction of β -Me-L-Trp in the MarE and variants mediated reaction in the presence of
	ascorbate
Figure S6	HRMS fragmentation pattern of product 1c from MarE reaction in the presence of
Figure S7	ascorbate
	The up-propionate interacts with GTGG motif containing JK-loop in human TDO
Figure S8	HPLC analysis for the reactions catalyzed by human TDO and variants on IPA (3)
Figure S9	HPLC chromatograms for the reactions catalyzed by TDO and the loop variants on L-Trp (2)
Figure S10	Comparisons of catalytic activities of TDO and the <u>GT</u> GGS-to- <u>SL</u> GGS variant on L-Trp (2)
Figure S11	Comparisons of catalytic activities of TDO and the $\underline{GT}GGS$ -to- $\underline{SL}GGS$ variant on the substrate
	of MarE, β-Me-L-Trp (1)
Figure S12	Near identical catalytic activity of MarE <u>SL</u> GGR-to- <u>GT</u> GGR variant on L-Trp (2) compared to
	wild-type MarE
Figure S13	The difference in the connectivity of the down-propionate between MarE and TDO
Figure S14	HPLC chromatograms for the reactions catalyzed by the TDO variants affecting the down-
	propionate on L-Trp (2)
Figure S15	HPLC analysis for the reaction products of IPA (3) as an alternative substrate
Figure S16	HPLC analysis for the reactions catalyzed by MarE and its loop variants on IPA (3)
Figure S17	The product formation profiles between 3b and 3c in the reactions promoted by human
	TDO, MarE, and their variants

References cited

DOI: 10.1002/anie.202510848

Materials and Methods

β-Me-L-Trp preparation

Synthesis of β-Me-L-Trp (1) followed the previously described method. [1] The Francis Arnold Lab generously shared the PfTrpB^{2B9} expression vector with us. Cell culture, gene expression, and protein purification were conducted as described. The purified PfTrpB^{2B9} was concentrated to 650 μM and stored at -80°C until use. In summary, indole (63.2 mg, 0.54 mmol) and L-threonine (595.8 mg, 5 mmol) were placed in a 20 mL vial. The solid mixture was then suspended in 3.5 mL of a 5% DMSO buffer solution containing 200 mM potassium phosphate (pH 8.0). A 15 mM stock solution of pyridoxal phosphate was prepared in water and subsequently added to the mixture to achieve a final concentration of 100 μ M. Purified PfTrpB^{2B9} was added to a final concentration of 160 μ M in a 5 mL reaction vial, then heated to 75°C in an oil bath while stirring. Following 18 h of reaction, the mixture was removed from heat, allowed to cool to room temperature, and the solids were subsequently pelleted via centrifugation. The crude supernatant was subjected to purification using a Teledyne ISCO Combiflash Rf system, which was equipped with a RediSep Gold C18 column. The column was washed with 2 column volumes (CVs) of water prior to performing an isocratic elution using a 50% methanol/water mixture. The solvent was subsequently removed under reduced pressure, resulting in the recovery of a lightly tan solid with a yield of 63.4%. Refer to Figure 2 in the main text for ¹H-NMR spectra of the purified β-Me-L-Trp (1). ¹H-NMR (300 MHz, D₂O) δ 7.67 (dt, J = 8.0, 1.1 Hz, 1H), 7.45 (dt, J = 8.0, 1.1 Hz, 18.2, 1.0 Hz, 1H), 7.27 (s, 1H), 7.19 (ddd, J = 8.2, 7.0, 1.3 Hz, 1H), 7.09 (ddd, J = 8.1, 7.0, 1.2 Hz, 1H), 3.86 (d, J = 6.6Hz, 1H), 3.63 (p, J = 7.1 Hz, 1H), 1.46 (d, J = 7.3 Hz, 3H).

Cloning, expression, and purification of MarE

A codon-optimized gene encoding the full-length MarE protein (amino acids 1 – 284) from *Streptomyces* sp. B9173 (UniProt ID: X2D878) was synthesized and obtained from GenScript. The synthesized MarE gene, located between Ndel and HindIII sites, was cloned into a modified pET-28a vector (Merck), named pET-28aTEV. This vector contains a Tobacco etch virus (TEV) protease cleavage site, which is intended for the removal of the N-terminal polyhistidine tag. The DNA sequences of the constructed expression vector plasmids were confirmed through DNA sequencing conducted by Eurofins Genomics.

MarE proteins with His-tags were produced in *E. coli* BL21 (DE3). Cells were cultured in Luria Bertani (LB) medium at 37°C with shaking at 220 rpm. The expression of the MarE gene was induced by adding 0.5 mM isopropyl-L-thio- β -D-galactopyranoside (IPTG) once the optical density at 600 nm (OD600) reached 0.8. The temperature was reduced to 20 °C, and the cells were cultured for an additional 16 to 20 h.

The harvested cells were resuspended in a solution of buffer A, which consists of 50 mM Tris-HCl, 200 mM NaCl, and 5% glycerol (pH 8.0) per gram of wet biomass. The cell membrane was disrupted using a sonicator (Thermo Fisher Scientific). A 300 mL cell suspension was stirred on wet ice with a 1 h pulse cycle of 1 sec on/1 sec off. Cell debris was removed by centrifugation at $34,000 \times g$ for 1 h at 4° C.

The supernatant containing His-tagged MarE was subsequently purified using immobilized metal affinity chromatography (IMAC) with a HisTrap column (Cytiva), pre-equilibrated with buffer A. The His-tagged protein was eluted using buffer B, which consists of buffer A and 500 mM imidazole. Histag removal was performed by treating the IMAC elution fraction with TEV protease during dialysis in buffer C, which contained 50 mM Tris-HCl, 50 mM NaCl, and 10 mM β -mercaptoethanol (pH 7.5) at 4 °C overnight. The tag-removed MarE protein was separated and collected using a HisTrap column with buffer A/B. The flow-through fraction was concentrated and desalted with a HiTrap Desalting column (Cytiva) in 50 mM HEPES-NaOH, 50 mM NaCl, 5% glycerol (pH 7.5). This buffer-exchanged, untagged MarE protein was used for heme reconstitution. The extinction coefficient at 280 nm (ϵ_{280}) for the untagged full-length MarE protein was calculated as 46,410 M⁻¹cm⁻¹ with a molecular weight of 31,996.77 Da using the Expasy ProtParam tool (https://web.expasy.org/protparam).

Heme reconstitution of MarE

A 4 mM stock solution of hemin chloride was freshly prepared by dissolving the compound in 50 mM NaOH. Hemin chloride, at a final concentration of 60 μ M, was added to 50 μ M of untagged MarE protein to achieve a hemin to protein ratio of 1.2:1 with gentle stirring. The reconstitution reaction was performed at room temperature for 3 h, followed by overnight incubation at 4°C. The reaction mixture was then centrifuged at 34,000 x g for 10 min at 4°C

DOI: 10.1002/anie.202510848 SI 3 of 28

RESEARCH ARTICLE

to remove precipitates. The supernatant was concentrated and desalted into a buffer containing 50 mM HEPES, 50 mM NaCl, and 5% glycerol (pH 7.5) to eliminate excess hemin. The heme-reconstituted protein was further concentrated and stored at -80°C. Through heme reconstitution, MarE achieved a heme occupancy of at least 70%, as determined by the heme extinction coefficient at 405 nm (ϵ_{405} = 169,198 M⁻¹cm⁻¹) using the pyridine hemochromagen method.

Pyridine hemochromagen assay

The quantity of heme was measured with the pyridine hemochromagen assay, which has an extinction coefficient (ϵ_{557}) of 34 mM⁻¹cm⁻¹ for its reduced form. ^[2]

Enzyme reaction

Enzyme reactions were prepared with the following components: $50~\mu\text{M}$ enzyme (heme), 20~mM or 1~mM sodium ascorbate, and 1~mM substrate ($\beta\text{-Me-L-Trp}$ (1), L-Trp (2), and IPA (3)) in Buffer A, which consists of 50~mM Tris-HCl, 200~mM NaCl, and 5% glycerol (pH 8.0). The reactions were conducted at a volume of $250~\mu\text{L}$ at room temperature for a duration of 16~h. Termination of the reactions involved filtration using a 10~kDa molecular weight cut-off (MWCO) centrifugal filter (Merck Millipore).

High-performance liquid chromatography (HPLC) coupled with mass spectrometry (LC-MS)

The use of a full wavelength detector in HPLC in our studies, including this and previous work, [3] reporting the full UV-vis spectrum of each reaction product, instead of a single-wavelength detector without the full spectrum of the reaction products, [4] was ultimately important in providing a complete description of the MarE reaction.

Each filtered reaction mixture was examined using a rapid separation system, specifically employing the Ultimate-3000SD HPLC from Thermo Fisher Scientific, which featured both a photodiode array detector and an ISQ EC mass spectrometer. For the analysis, $20~\mu$ L of each sample was injected into an InertSustain C18 column with a particle size of $5~\mu$ m and dimensions of 4.6~l.D.~x~100~mm by GL Sciences Inc. The elution process was conducted isocratically with a solvent blend of water, acetonitrile, and 0.1% formic acid at a flow rate of 1.0~mL/min. Due to varying solubilities, the following acetonitrile concentrations were utilized: 6.0% for β -Me-L-Trp (1), 1.7% for L-Trp (1), and 1.7% for IPA (1). Each elution run lasted 1.00 min.

High resolution mass spectrometry (HRMS)

High-resolution mass spectra were acquired using a maXis plus quadrupole-time of flight mass spectrometer equipped with an electrospray ionization source (Bruker Daltonics) in positive ionization mode. Liquid chromatography fraction samples were introduced at a flow rate of 3 μ L/min via a syringe pump. Key parameters for the ion source were set as follows: capillary voltage at 3500 V, endplate offset at –500 V, nebulizer gas pressure at 0.4 bar, dry gas flow at 4.0 L/min, and source temperature at 200°C. Mass spectra were recorded at one scan per second over a range of 50-1500 m/z, and averaged over one minute. The Compass Data Analysis software version 4.3 (Bruker Daltonics) was used to process all mass spectra.

Scaled-up enzyme reaction and product purification for NMR

In order to accumulate sufficient product for NMR analysis of the dioxygenated products of β -Me-L-Trp (1), 15 - 25 mL reactions were carried out with 180 μ M MarE reduced with 1.1 equivalents of dithionite prepared in anaerobic buffer using the Schlenk line and gas-tight Hamilton syringes. The substrate β -Me-L-Trp (1) was dissolved in oxygensaturated buffer to a final 2 mM concentration and titrated 1 mL at a time into the reduced MarE mixture while gently stirring the mixture on ice. The resulting reaction mixture was allowed to proceed at 4°C. After 16 h, the enzyme was removed using a 10 kDa filter, and the filtrate was lyophilized to a beige, white solid to prepare for purification. Approximately 320 mL of reaction was needed to generate a sufficient amount of each product for NMR analysis.

NMR analysis of the reaction products collected via preparative HPLC and lyophilization

DOI: 10.1002/anie.202510848 SI 4 of 28

RESEARCH ARTICLE

A separate semi-preparative Ultimate-3200BX HPLC with a multiple wavelength MWD-3000 detector from Thermo Fisher Scientific was used to repeatedly pool the reaction products for NMR analyses. A Labconco Lyophilizer System, FreeZone 2.5 Liter -84 °C Benchtop Freeze Dryer, was used to aid the sample preparation.

The white solid was dissolved in 3 mL nanopure water and injected into the semi-preparative HPLC equipped with a 250 mm x 20 mm internal diameter column (Thermo Fisher Scientific) and a fraction collector. The fractions for each product were collected in separate 50 mL conical tubes and lyophilized to prepare for purification on the analytical Ultimate-3000SD HPLC rapid separation system equipped with a photodiode array detector. Each product fraction was dissolved in 500 μ L nanopure water and injected into the analytical HPLC. Each product was collected in 15 mL conical tubes and lyophilized. NMR samples were made in D₂O using thick-walled NMR tubes and analyzed on a Bruker 500 MHz Avance III equipped with a 5 mm Prodigy CryoProbe.

NMR spectra were acquired on a Bruker 500 MHz Avance III HD spectrometer operating at 11.7 T. TopSpin 3.5pl6 was used for data processing.

DOI: 10.1002/anie.202510848 SI 5 of 28

Table S1. The codon-optimized DNA sequence of MarE and primers used in this study for MarE and human TDO mutagenesis studies

Codon-optimized DNA sequence of MarE

ATGAAGCGTAGCCTGAACCCGGACGAACCGAACGCGCTGCTGAGCTACGACTTCGATCGTGGCAGCAACT ATGAGAACGTGCTGCATCTGACCGATGCGCTGGGTGCGCTGGTTCCGGAGAGCGAAACCGAGCACCCGGA TCAGCGTTTCTTTCAAGTTACCCACCTGATCACCGAATACGCGTGGGTGCAGGTTCACTATGAGCTGCGT CGTGCGATTGGCCACCTGGACGAAGATCGTTACCACCAAGCGGTTCGTATGTTTGACCGTGCGACCGGTC TGAGCGAGGTGACCGTTCAGGCGGTGCGTCTGCTGACCGATCACCTGCCGCAACACAGCCTGCTGATGAT GCGTAACGCGCTGCCGGAAGATGCGACCGGTCTGGATAGCCCGGGTTACCGTAACCTGCGTCGTGTGGCG CGTCCGGTTTGGAAAGCGTATGAACAAGCGGTGGAGCGTGCGGGTCTGAGCCTGCAAGACGTTATCGCGC AGCAAGACGATGGCTATGATGGTCCGCGTAGCGGTGGCAGCCAGAGCCTGGCGCTGGTGCGTGAGGCGAT GCTGCGTCTGGACGGCAGCGTTCTGGGTTGGAAGCACCACCTGATTATGGTGTGGAGCCAGCTGGGT GGCCAACCGGGTCTGCGTAAGGGTAACGAGGAAGGCGACGATGGTCTGGAACTGCCGCAGAGCCTGGGTG GCCGTAGCCTGGCGACCCTGGAGGCGCGTAGCCAACTGGCGCTGTTTCCGGAACTGTGGCGTGCGGCGGA GGATGCGTACTGGCTGCTGGGTACCCGTCATGACACCGATGCGCCGGTGCGTGGCGGTAACGGTTGC **CCGGTTCAGCACTAA**

Mutagen	2129	nrım	ers
Widtagen	C313	P11111	C 1 3

Mutagenesis primers	
MarE L232T	AACTGCCGCAGAGC <u>ACG</u> GGTGGCCGTAGCC
MarE S231G on L232T	AACTGCCGCAG <u>GGC</u> ACGGGTGGC
MarE R235S (SLGG <u>R</u> -to-SLGG <u>S</u>)	AGCCTGGGTGGC <u>TCT</u> AGCCTGGCGAC
MarE R235S on <u>SL</u> GGR-to- <u>GT</u> GGR	GCACGGGTGGC <u>TCT</u> AGCCTGGCGA
TDO <u>GT</u> GGS-to- <u>SL</u> GGS	TGGGCAGCAAAGCT <u>AGCCTC</u> GGTGGTTCCTCA
TDO GTGG <u>S</u> -to-GTGG <u>A</u>	TGGCACCGGTGGT <u>GCC</u> TCAGGCTATCA
TDO G <u>TG</u> GS-to-G <u>PP</u> GS	AGCAAAGCTGGC <u>CCCCCT</u> GGTTCCTCAGGC
TDO GTGGS-to-G_GGS	AGCAAAGCTGGCGGTGGTTCCTCA
TDO R159A	TCCAGAGTTTGCAATTC <u>GCA</u> CTATTAGAAAACAAGA
TDO Y350F	TTCCTCAGGCTATCAC <u>TTC</u> CTGCGATCAACTGTGA
TDO R325A	ACTGATGACCAAATGG <u>GCA</u> TATAACCATGTGTGC

The forward primers for mutagenesis are provided, and the reverse primers are the reverse complement of these forward primers. Site-directed mutagenesis was conducted employing the QuickChange PCR protocol (Agilent Technologies).

DOI: 10.1002/anie.202510848

Table S2. $^1\text{H-NMR}$ (500 MHz, D₂O) and $^{13}\text{C-NMR}$ (126 MHz, D₂O) for MarE product **1b**.

1' 2' 3.93 (d, $J = 4.8 \text{ Hz}$, 1H) 56.42 3' 4.19 (td, $J = 7.3$, 4.5 Hz, 1H) 42.65 4' 1.25 (d, $J = 7.1 \text{ Hz}$, 3H) 13.25 1 2 206.40 3	
3' 4.19 (td, <i>J</i> = 7.3, 4.5 Hz, 1H) 42.65 4' 1.25 (d, <i>J</i> = 7.1 Hz, 3H) 13.25 1 2	
4' 1.25 (d, <i>J</i> = 7.1 Hz, 3H) 13.25 1 2 206.40	
1 2 206.40	
2 206.40	
3 165.53	
3a	
4 8.03 (d, <i>J</i> = 8.3 Hz, 1H) 123.88	
5 7.32 (t, <i>J</i> = 7.7 Hz, 1H) 125.49	
6 7.60 (t, <i>J</i> = 7.8 Hz, 1H) 134.40	
7 7.88 (d, <i>J</i> = 7.9 Hz, 1H) 130.17	
7a	

Table S3. 1 H-NMR (500 MHz, D₂O) and 13 C-NMR (126 MHz, D₂O) for MarE product **1b₁**.

Label	δ_{H}	$\delta_{\rm C}$
1'		
2'	4.03 (d, <i>J</i> = 7.0 Hz, 1H)	56.52
3'	2.73 (p, <i>J</i> = 7.2 Hz, 1H)	40.10
4'	0.67 (d, <i>J</i> = 7.3 Hz, 3H)	11.59
1		
2		
3		
3a		
4	7.38 (d, <i>J</i> = 7.5 Hz, 1H)	123.83
5	7.13 (t, <i>J</i> = 7.6 Hz, 1H)	123.67
6	7.31 (t, <i>J</i> = 7.7 Hz, 1H)	130.41
7	6.94 (d, <i>J</i> = 8.2 Hz, 1H)	110.90
7a		

Table S4. ¹H-NMR (500 MHz, D₂O) and ¹³C-NMR (126 MHz, D₂O) for MarE product **1a₂**.

Label	δн	δ_{C}	
1'		172.34	
2'	3.27 (d, <i>J</i> = 12.3 Hz, 1H)	64.26	
3'	2.62 (dq, <i>J</i> = 13.5, 6.9 Hz, 1H)	47.13	
4'	1.19 (d, <i>J</i> = 6.9 Hz, 3H)	11.50	
1			
2	5.37 (s, 1H)	82.93	
3		90.15	
3a		125.51	
4	7.33 (d, <i>J</i> = 7.6 Hz, 1H)	126.61	
5	6.88 (t, <i>J</i> = 7.5 Hz, 1H)	131.01	
6	7.24 (t, <i>J</i> = 7.7 Hz, 1H)	120.04	
7	6.76 (d, <i>J</i> = 8.0 Hz, 1H)	110.85	
7a		149.71	

Table S5. ¹H-NMR (500 MHz, D₂O) and ¹³C-NMR (126 MHz, D₂O) for MarE product **1a₁**.

Label	δн	δς
1'		172.24
2'	3.82 (d, <i>J</i> = 8.6 Hz, 1H)	66.08
3'	2.58 (p, <i>J</i> = 7.3 Hz, 1H)	45.52
4'	1.30 (d, <i>J</i> = 7.1 Hz, 3H)	11.45
1		
2	5.26 (s, 1H)	84.13
3		88.27
3a		129.52
4	7.29 (d, <i>J</i> = 7.5 Hz, 1H)	123.22
5	6.86 (t, <i>J</i> = 7.5 Hz, 1H)	120.77
6	7.22 (t, <i>J</i> = 7.7 Hz, 1H)	130.80
7	6.75 (d, <i>J</i> = 8.0 Hz, 1H)	111.41
7a		147.59

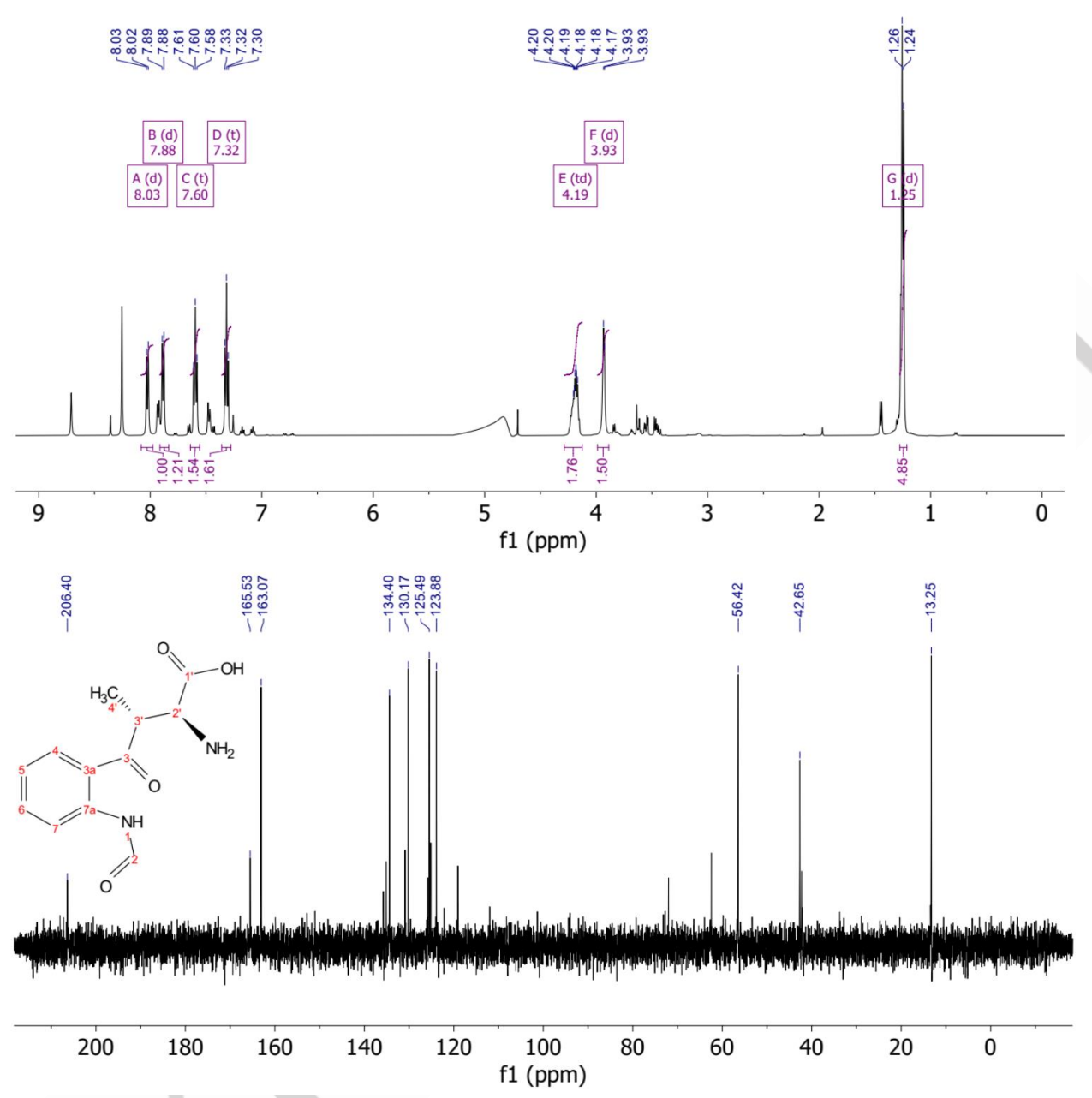


Figure S1. ¹H- and ¹³C-NMR of product **1b** in D₂O from the MarE reaction with dioxygen.

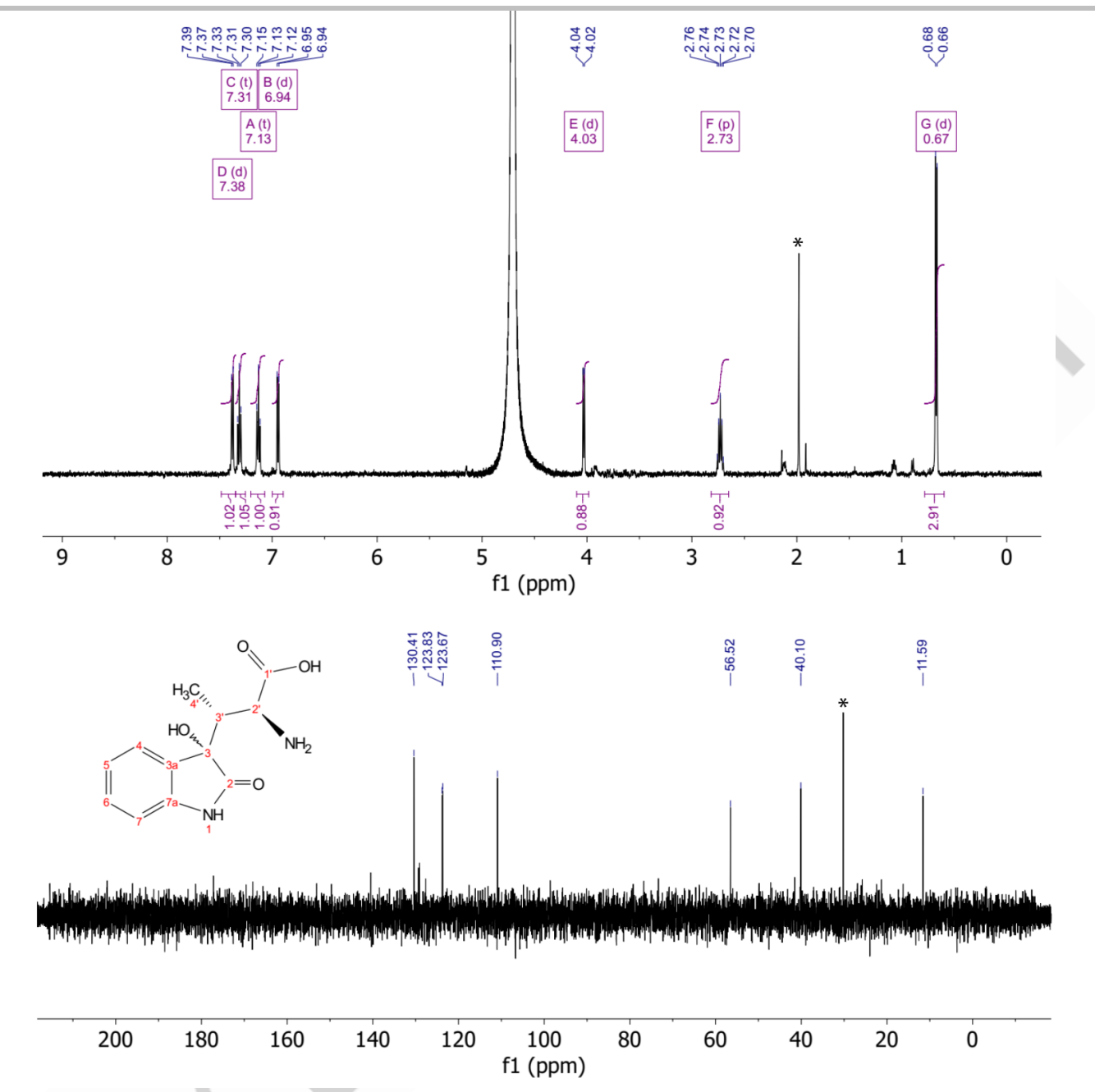


Figure S2. 1 H- and 13 C-NMR of product $1b_{1}$ in D_{2} O from the MarE reaction with dioxygen (* denotes an impurity not associated with the structure of the product). The quaternary carbons are not resolved due to low S/N.

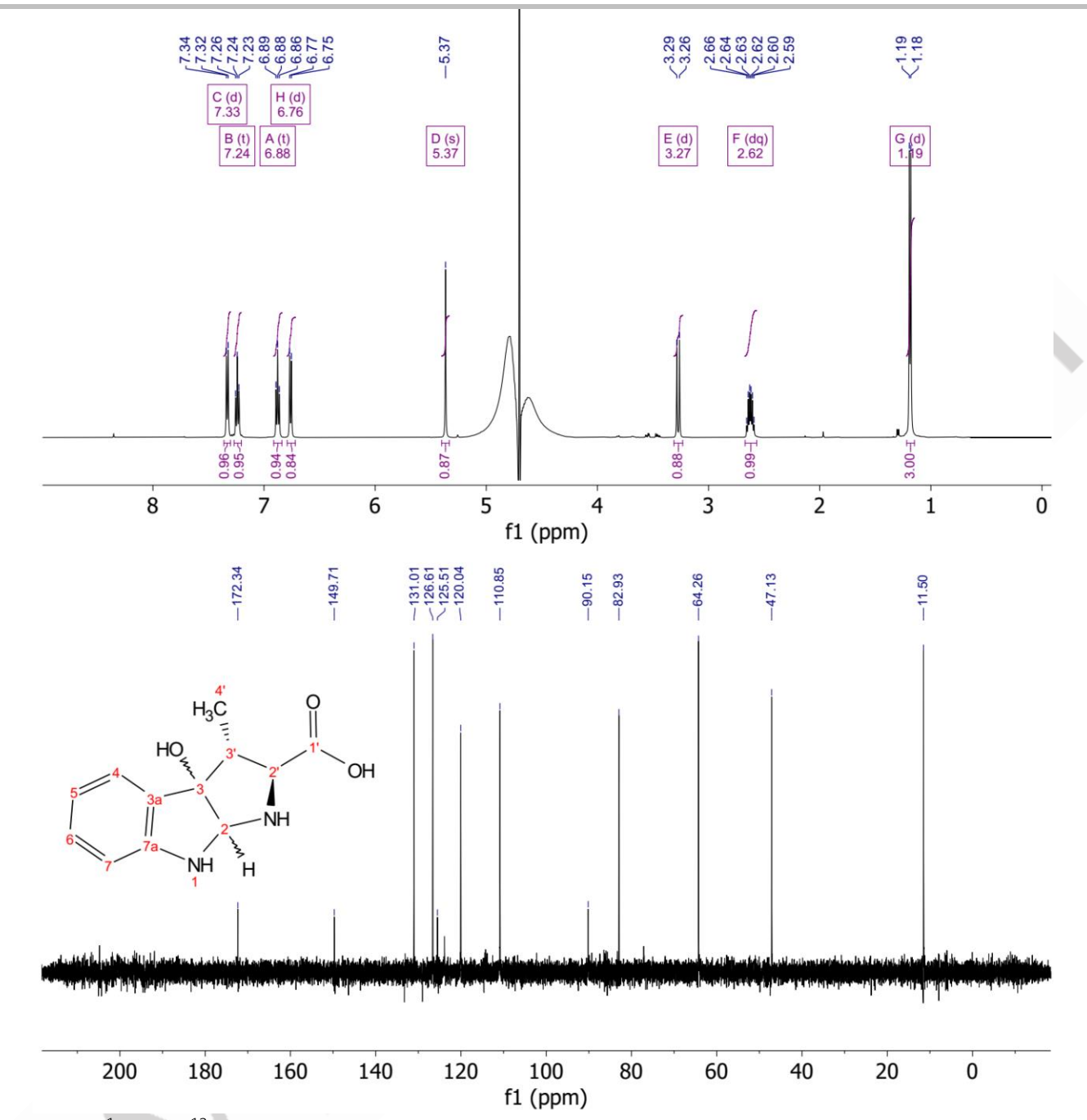


Figure S3. ¹H- and ¹³C-NMR of product **1a₂** in D₂O from the MarE reaction with dioxygen.

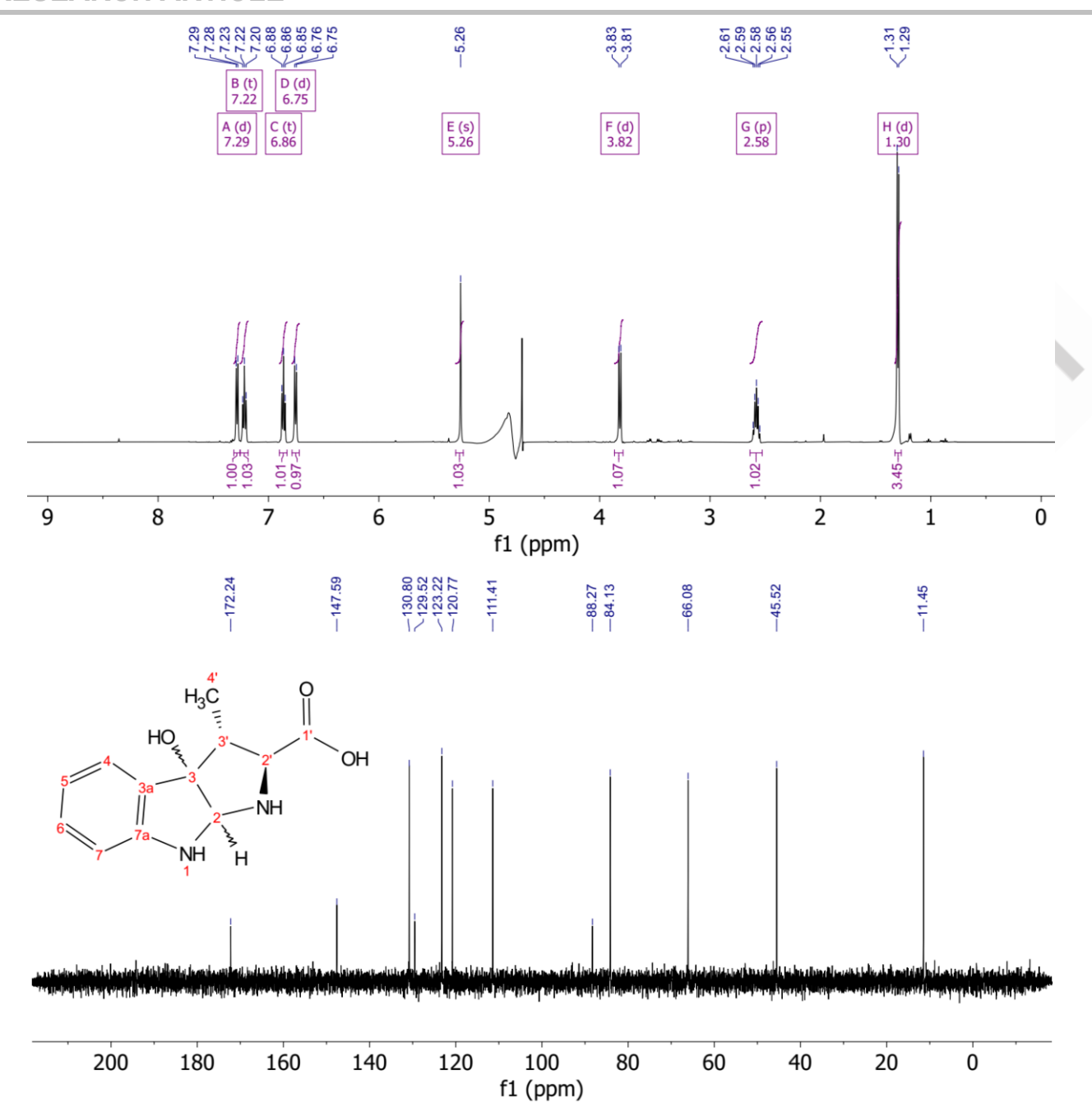


Figure S4. 1 H- and 13 C-NMR of product $1a_{1}$ in D_{2} O from the MarE reaction with dioxygen.

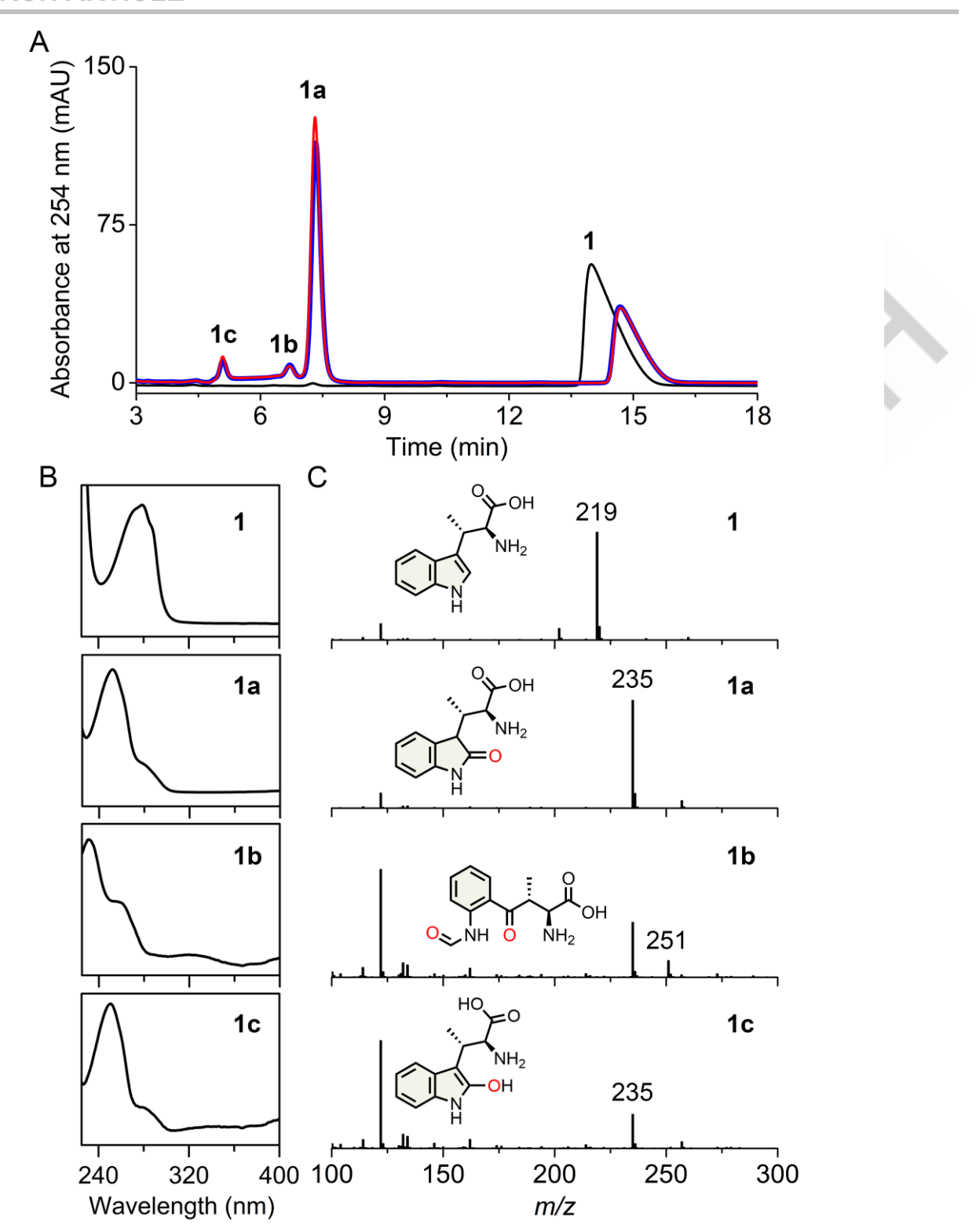


Figure S5. Reaction of β-Me-L-Trp in the MarE and variants mediated reaction in the presence of ascorbate. (A) The reactions catalyzed by MarE wild-type (blue trace) and <u>SL</u>GGR-to-<u>GT</u>GGR variant (red trace) with β-Me-L-Trp (**1**, black trace) and ascorbate in the presence of O_2 were analyzed by HPLC. Reactions were carried out using enzyme (50 μ M heme), ascorbate (20 mM), and β-Me-L-Trp (1 mM). (B) UV-vis spectra of substrate **1** and products **1a**, **1b**, and **1c**. (C) Mass spectra of the peaks from the HPLC elution profile and their chemical structures.

DOI: 10.1002/anie.202510848 SI 15 of 28

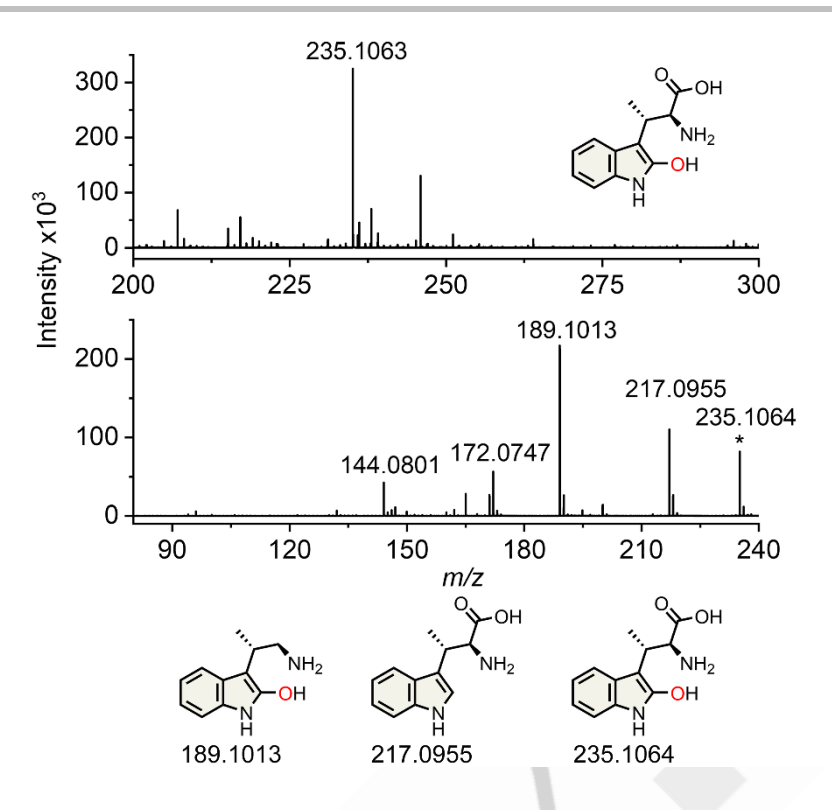


Figure S6. HRMS fragmentation pattern of product **1c** from MarE reaction in the presence of ascorbate. Asterisk mark (*) denotes the parent ion for fragmentation.

DOI: 10.1002/anie.202510848

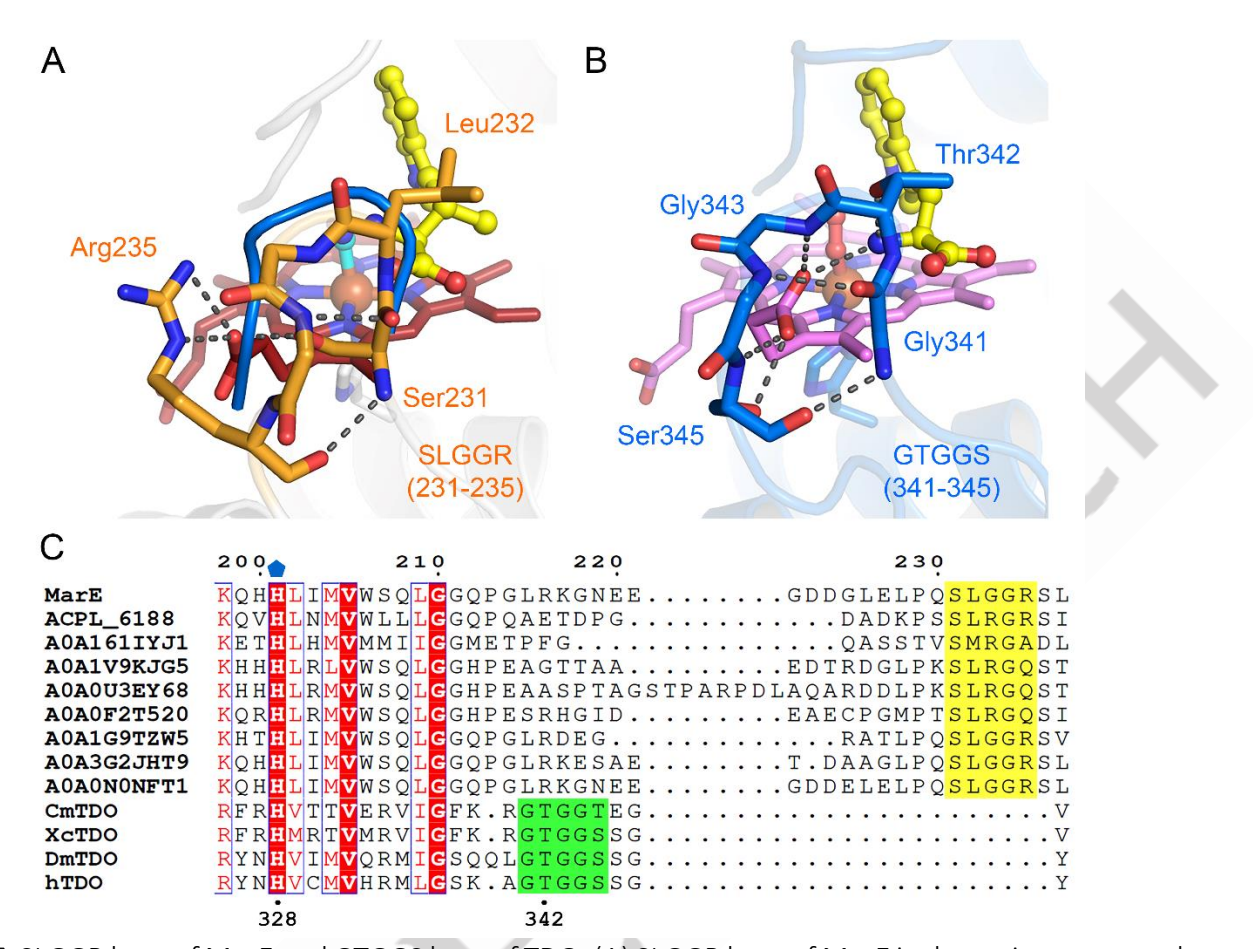


Figure S7. SLGGR loop of MarE and GTGGS loop of TDO. (A) SLGGR loop of MarE is shown in orange carbon color stick model with cyanide (cyan)-bound heme (dark red) and β -Me-L-Trp (yellow) (9CA3.pdb). GTGGS loop of TDO (blue) is overlaid with SLGGR loop. (B) GTGGS loop of TDO is shown in stick model (blue) with O2 (red)-bound heme (pink) and L-Trp (yellow) (5TI9.pdb). (C) Segment of multiple sequence alignments of MarE and TDO from various origins. Numbering at the top corresponds to MarE, while numbering at the bottom pertains to TDO. A blue solid pentagon denotes the axial heme ligand. Green boxes indicate the GTGGS loop in TDOs, and yellow boxes highlight the corresponding SLGGR in MarE.

DOI: 10.1002/anie.202510848

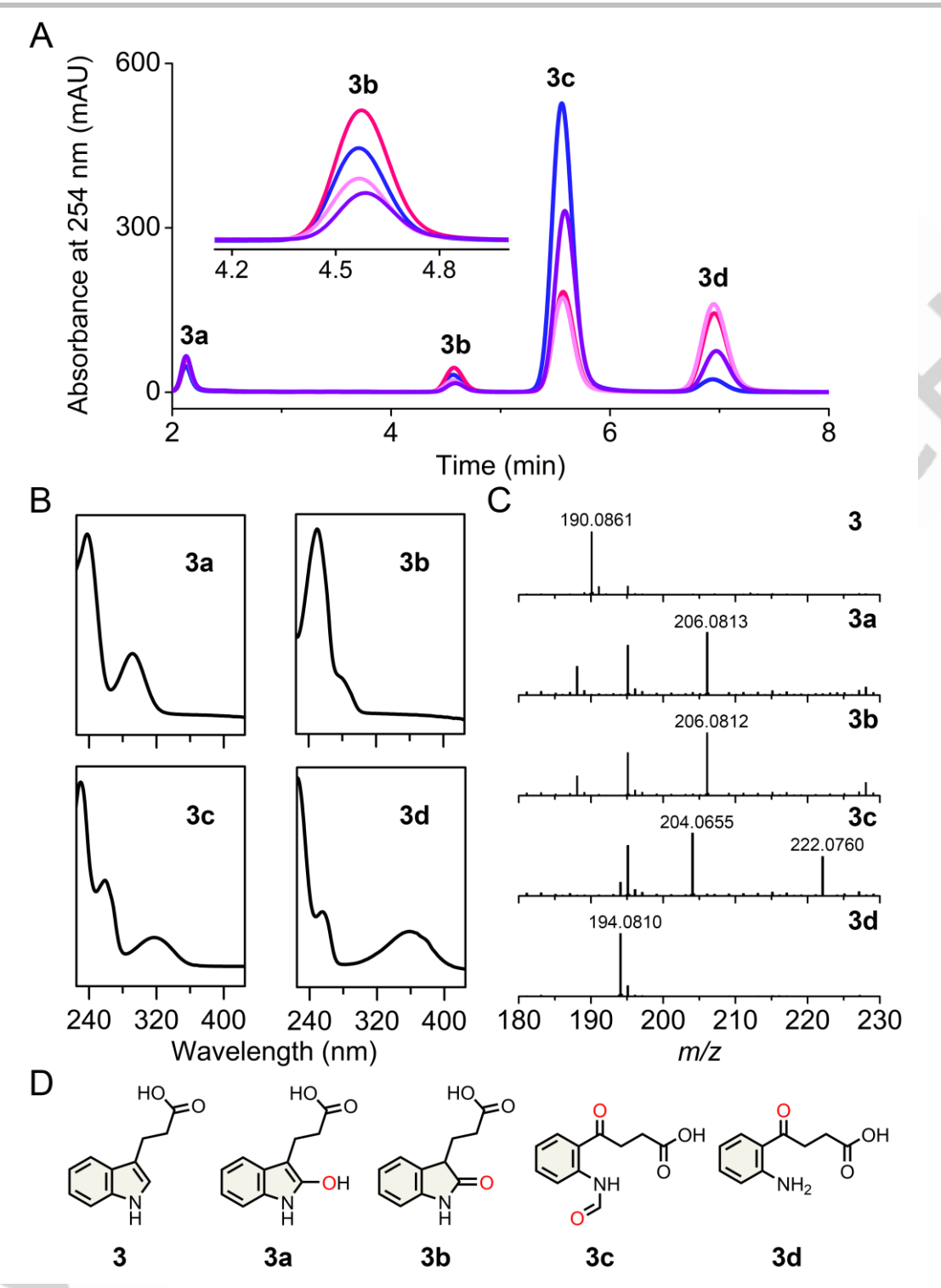


Figure S8. HPLC analysis for the reactions catalyzed by human TDO and variants on IPA (3). Chromatograms are shown for wild-type TDO (), GTGGS-to-GTGGA TDO (), GTGGS-to-GPPGS TDO (), and GTGGS-to-G_GGS TDO (). The inset is the zoomed-in view for peak 3b. Each reaction was carried out using enzyme (50 μ M), IPA (1 mM), and ascorbate (20 mM). (B) UV-vis spectra of peaks 3a, 3b, 3c, and 3d. (C) HRMS analysis of LC fractions. Calculated m/z values with HRMS errors in ppm are as follows: 3 (C₁₁H₁₁NO₂), 190.0863 (1.05 ppm); 3a and 3b (C₁₁H₁₁NO₃), 206.0812 (0.48 and 0 ppm); 3c (C₁₁H₁₁NO₄), 222.0761 (0.45 ppm); 3d (C₁₀H₁₁NO₃), 194.0812 (1.03 ppm). The UV-vis spectrum of 3d has a peak centered at 358 nm and m/z value of 194.0810, consistent with a loss of a formyl group. (D) Chemical structures of IPA (3) and its oxygenation products.

DOI: 10.1002/anie.202510848 SI 18 of 28

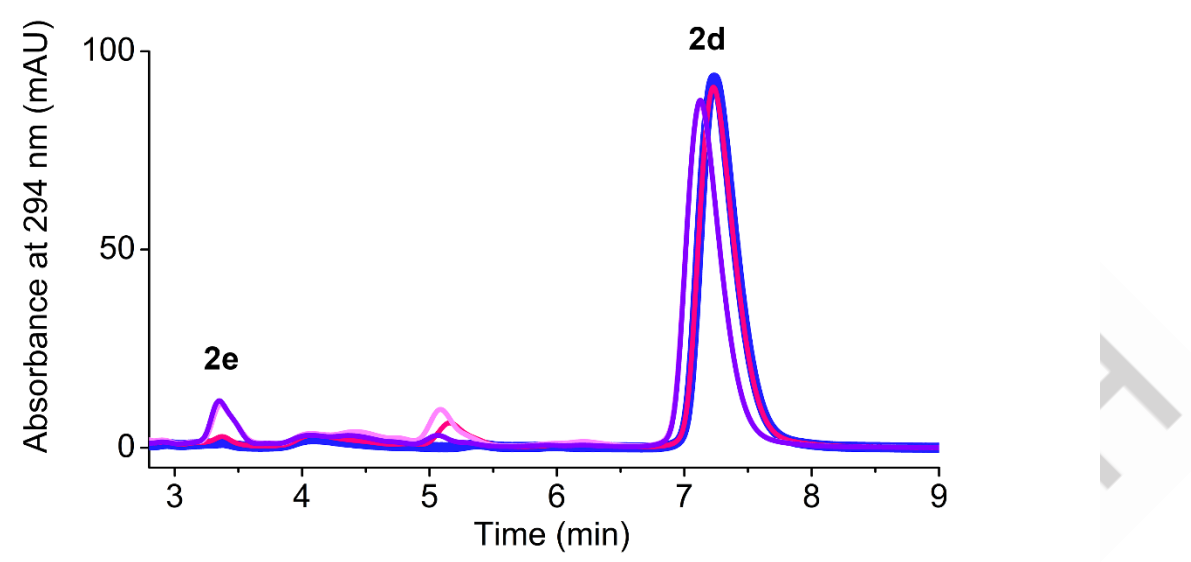


Figure S9. HPLC chromatograms for the reactions catalyzed by TDO and the loop variants on L-Trp (2). Wild-type TDO (), GTGGS-to-GTGGA TDO (), and GTGGS-to-G_GGS TDO (), and GTGGS-to-G_GGS TDO (). Each reaction was carried out using enzyme (30 μ M heme), L-Trp (1 mM), and ascorbate (20 mM).



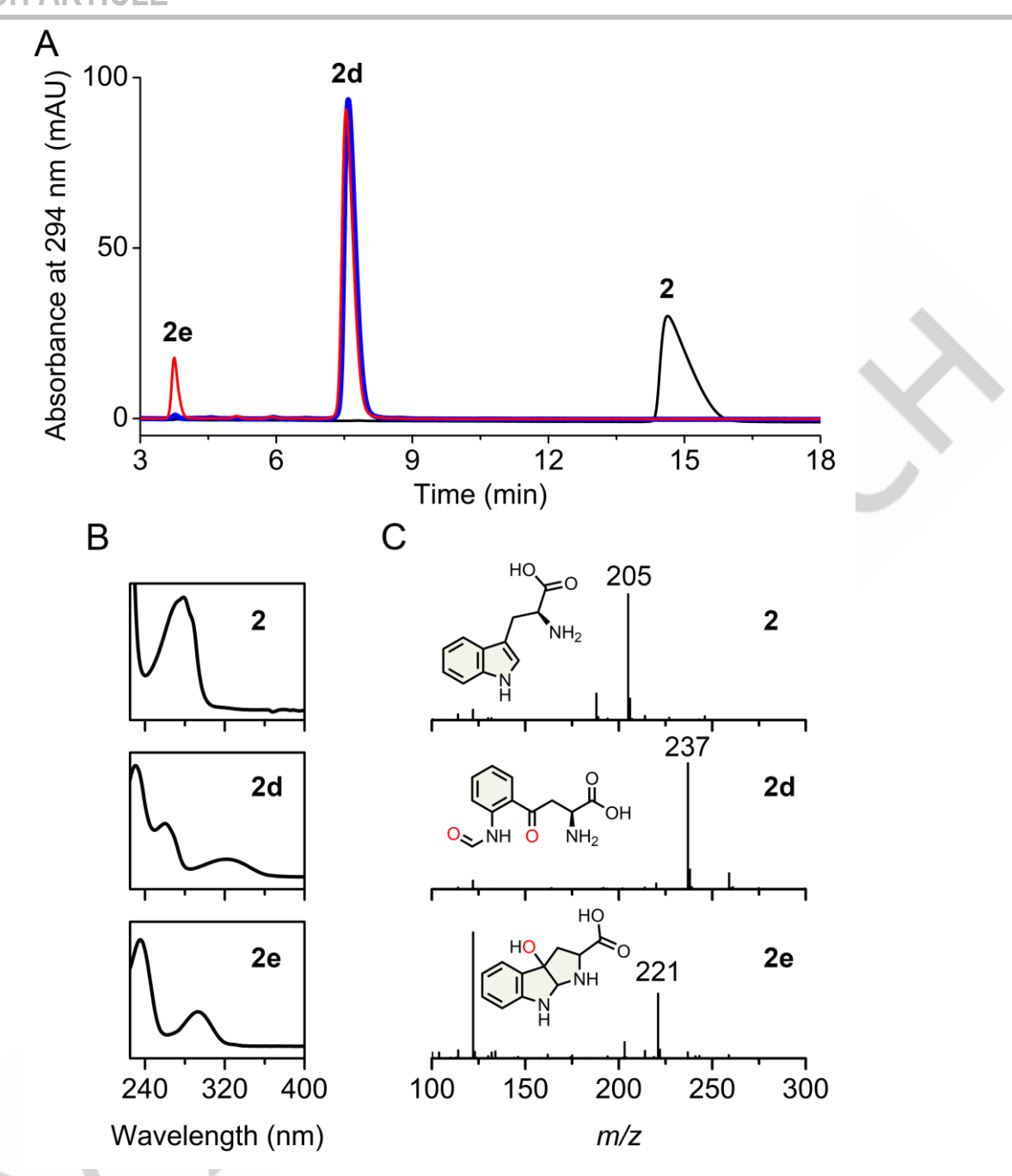


Figure S10. Comparisons of catalytic activities of TDO and the $\underline{GT}GGS$ -to- $\underline{SL}GGS$ variant on L-Trp (2). (A) The reactions catalyzed by wild-type TDO (blue trace) and $\underline{GT}GGS$ -to- $\underline{SL}GGS$ variant (red trace) with L-Trp (2, black trace) were analyzed by HPLC. Reactions were carried out using enzyme (50 μ M heme), ascorbate (1 mM), and L-Trp (1 mM). (B) UV-vis spectra of peaks from the HPLC elution profile. (C) Mass spectra of the peaks from the HPLC elution profile and their chemical structures.

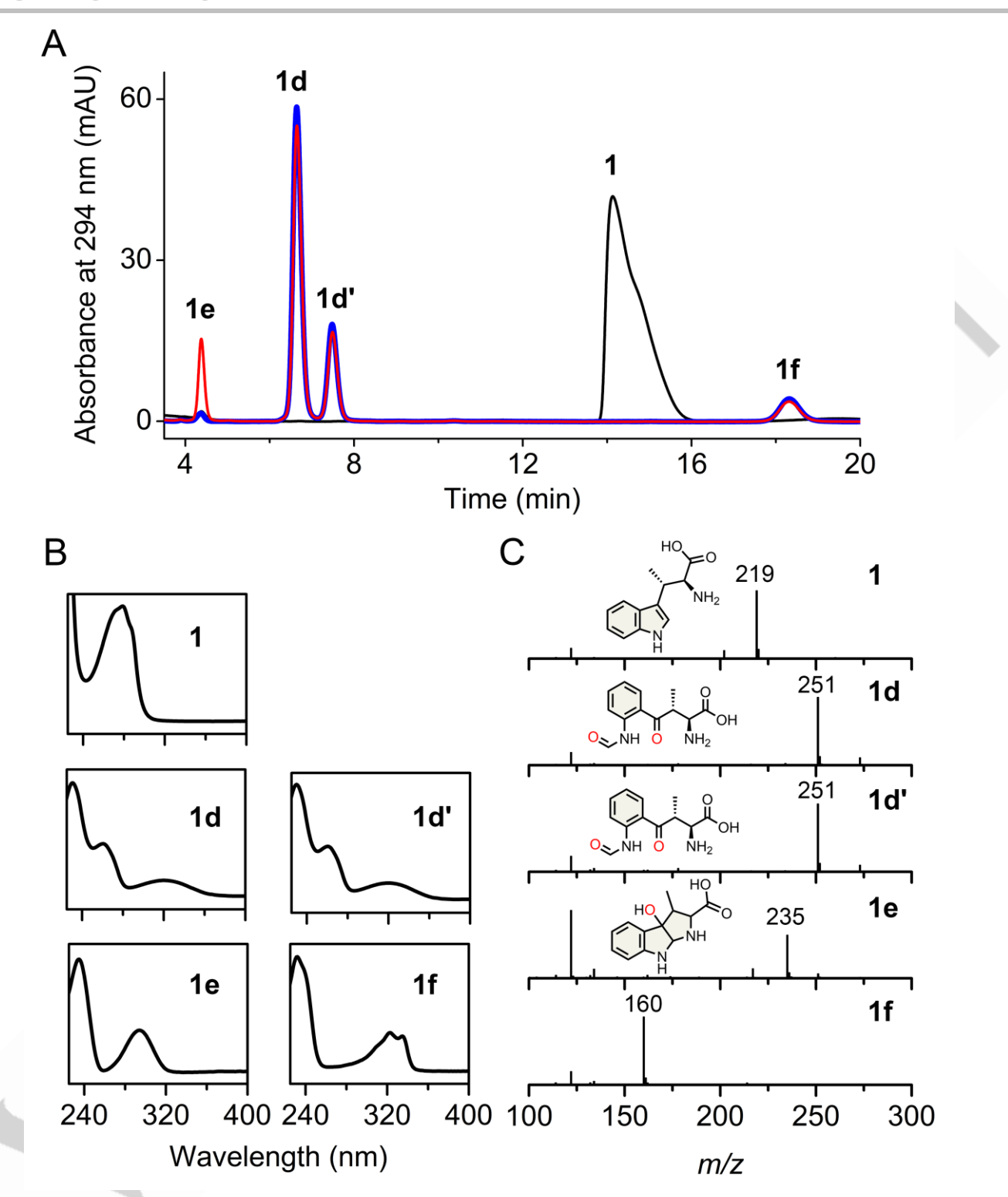


Figure S11. Comparisons of catalytic activities of TDO and the <u>GT</u>GGS-to-<u>SL</u>GGS TDO variant on the substrate of MarE, β-Me-L-Trp (**1**). (A) The reactions catalyzed by wild-type TDO (blue trace) and <u>GT</u>GGS-to-<u>SL</u>GGS TDO variant (red trace) with β-Me-L-Trp (**1**, black trace) were analyzed by HPLC. Reactions were carried out using enzyme (50 μ M heme), ascorbate (1 mM), and β-Me-L-Trp (1 mM). (B) UV-vis spectra of the elute from the HPLC separation profile. (C) Mass spectra of the peaks from the HPLC elution profile and their chemical structures.

DOI: 10.1002/anie.202510848 SI 21 of 28

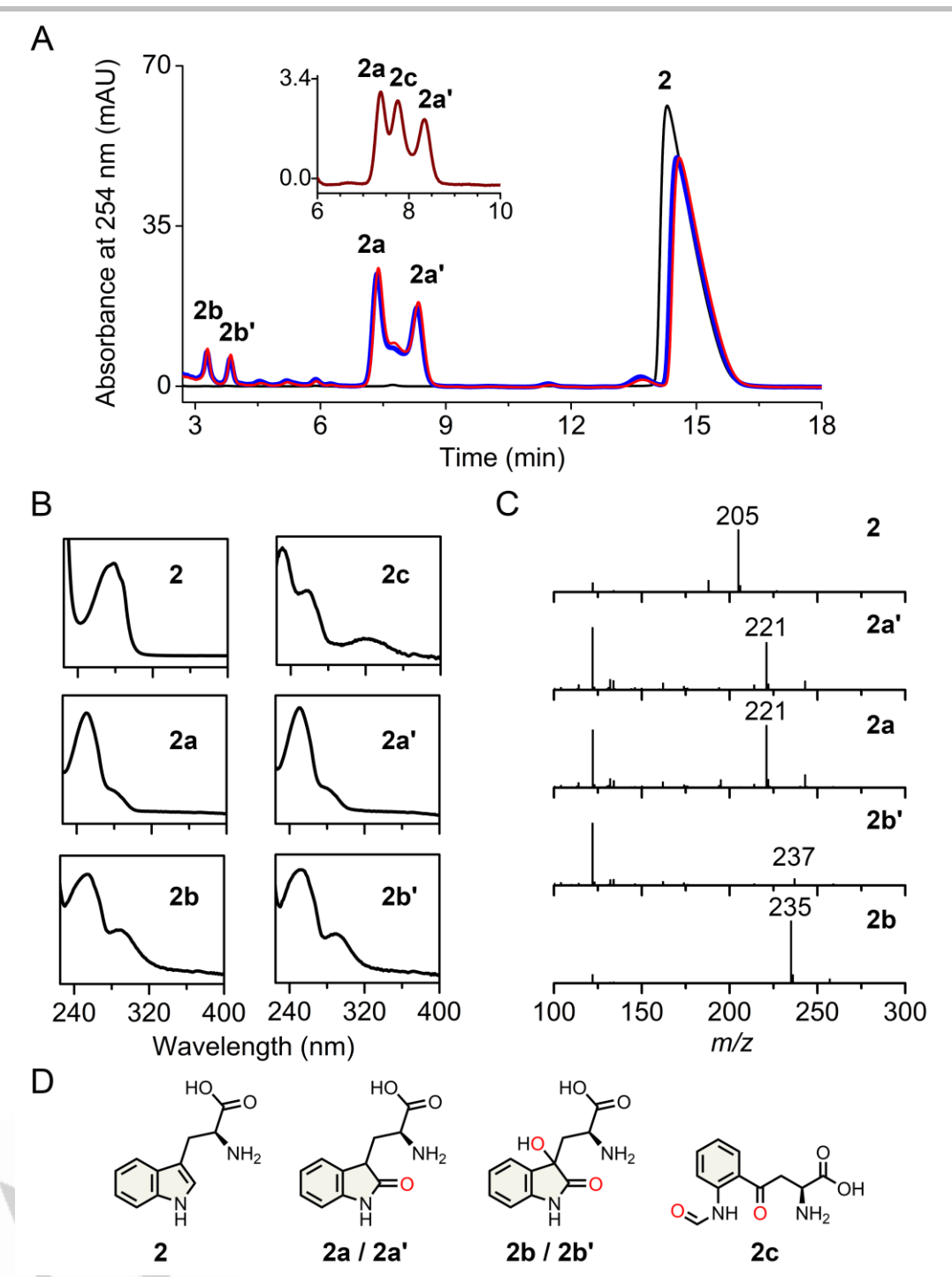


Figure S12. Near identical catalytic activity of MarE and the <u>SL</u>GGR-to-<u>GT</u>GGR variant on L-Trp (2). (A) The reactions catalyzed by MarE wild-type (blue trace) and <u>SL</u>GGR-to-<u>GT</u>GGR variant (red trace) with L-Trp (2, black trace) were analyzed by HPLC. Reactions were carried out using enzyme (50 μM heme), ascorbate (20 mM), and L-Trp (1 mM). Inset is the HPLC chromatogram of MarE <u>SL</u>GGR-to-<u>GT</u>GGR variant with lower concentration of ascorbate (1 mM) (dark red trace). (B) UV-vis spectra of peaks from the HPLC elution profile. (C) Mass spectra of the peaks from the HPLC elution profile. (D) Chemical structures of L-Trp (2) and its oxygenated products by MarE. When less ascorbate (1 mM) was used, eluant 2c emerged between 2a and 2a' with spectral features similar to 1b (Figure 2). The MS detection of 2c was unsuccessful due to its significantly low intensity. Products 2b and 2b' share similar UV-vis features with an absorption maximum centered at 294 nm and a feature centered at 253 nm, which are distinct from those of 2a and 2a'. The m/z values of 2b and 2b' were 235 and 237.

DOI: 10.1002/anie.202510848 SI 22 of 28

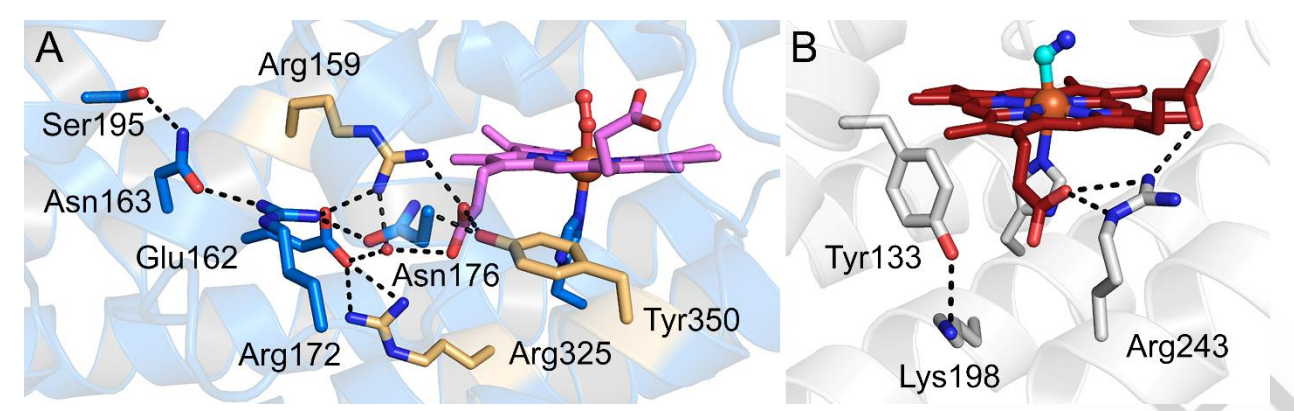


Figure S13. The difference in the connectivity of the down-propionate between MarE and TDO. (A) Surrounding residues near the down-propionate in TDO. Direct interactions between the down-heme-propionate and Arg159, Tyr350, and Arg325 are presented (5TI9.pdb). (B) Residues near the down-propionate in MarE (9CA3.pdb). Interactions within 3.2 Å are presented with dotted lines.



DOI: 10.1002/anie.202510848 SI 23 of 28

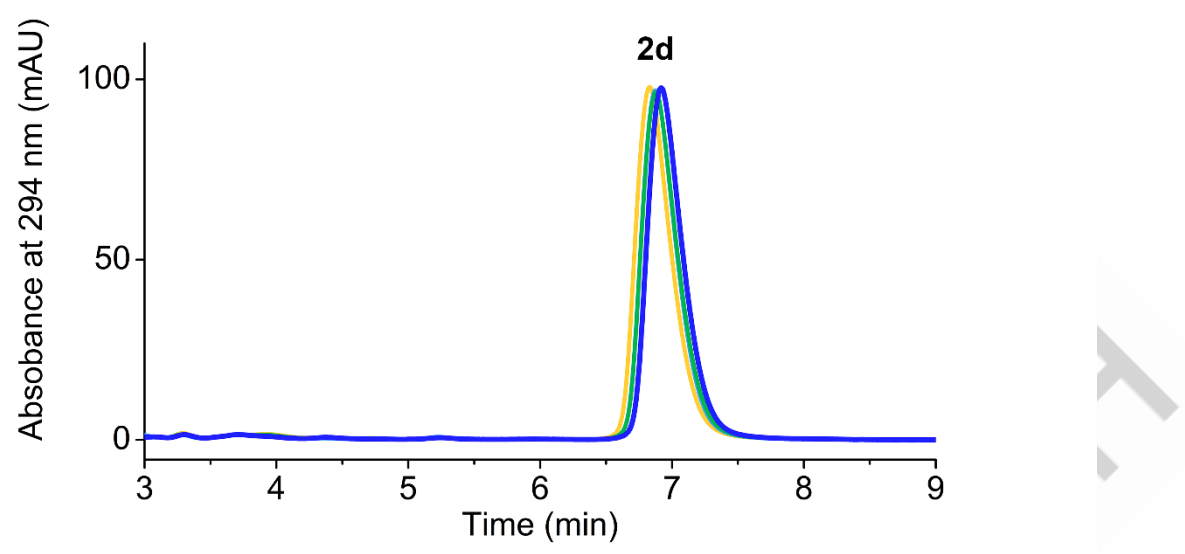


Figure S14. HPLC chromatograms for the reactions catalyzed by TDO variants affecting the down-propionate on ι -Trp (2). The wild-type TDO (______), R325A TDO (______), R159A TDO (______), and Y350F TDO (______). Each reaction was carried out using the enzyme (15 μ M heme), ι -Trp (1 mM), and ascorbate (20 mM).



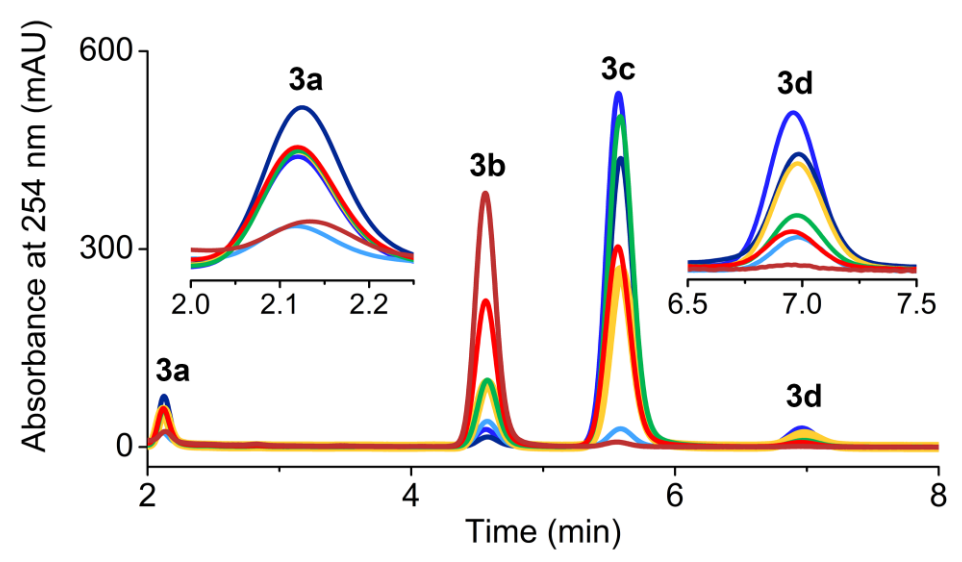


Figure S15. HPLC analysis for the reaction products of IPA (3) as an alternative substrate. (A) Chromatograms are shown for wild-type TDO (______), GTGGS-to-SLGGS TDO (______), R325A TDO (______), R159A TDO (______), wild-type MarE (______), and SLGGR-to-GTGGR MarE (______).



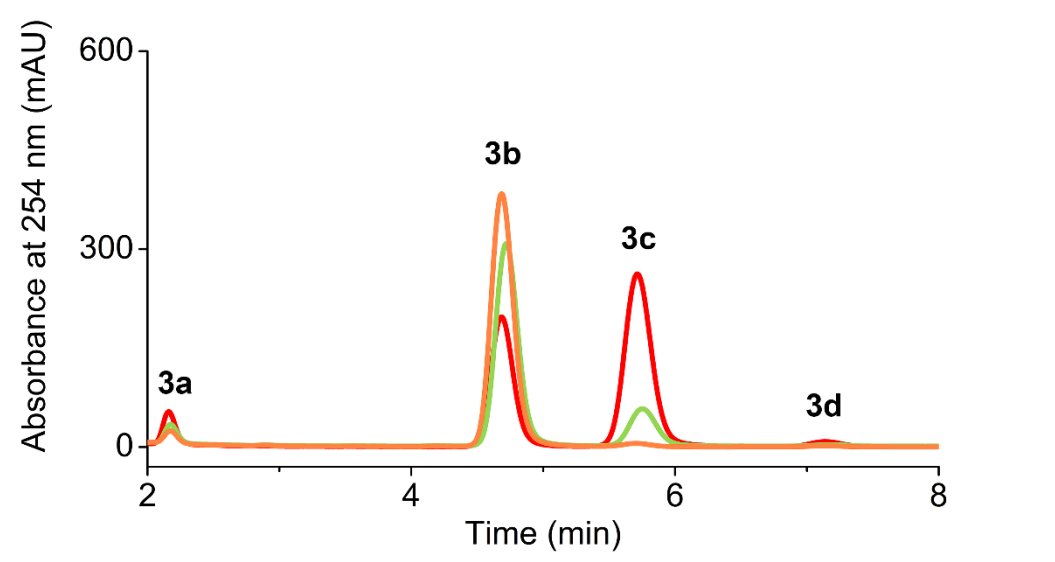


Figure S16. HPLC analysis for the reactions catalyzed by MarE and its loop variants on IPA (3). Chromatograms are shown for wild-type MarE ($\blacksquare\blacksquare\blacksquare$), SLGGR-to-SLGGS MarE ($\blacksquare\blacksquare\blacksquare$), and SLGGR-to-GTGGS MarE ($\blacksquare\blacksquare\blacksquare$). Each reaction was carried out using enzyme (50 μ M), IPA (1 mM), and ascorbate (20 mM).



DOI: 10.1002/anie.202510848 SI 26 of 28

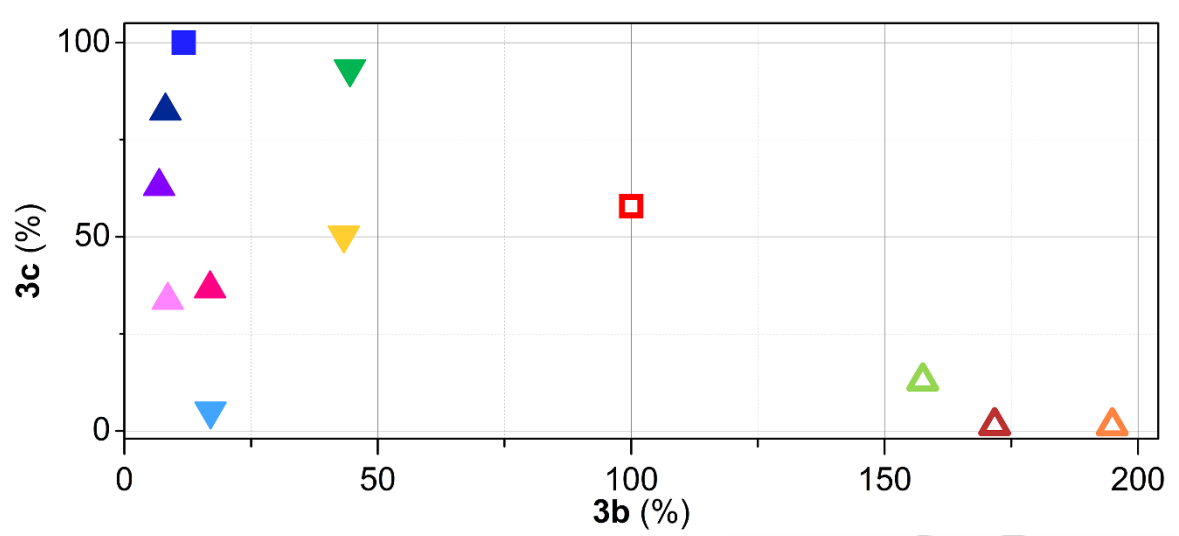


Figure S17. The product formation profiles between 3b and 3c in the reactions promoted by MarE, human TDO, and their variants. Solid and open symbols represent TDO and MarE, respectively. Square symbols stand for wild-type enzymes. Up triangles denote loop variants. Down triangles are variants for the down-propionate, which are wild-type MarE (\square), SLGGR-to-GTGGR MarE (\triangle), SLGGR-to-SLGGS MarE (\triangle), and SLGGR-to-GTGGS MarE (\triangle), wild-type TDO (\square), GTGGS-to-SLGGS TDO (\triangle), R325A TDO (\square), R159A TDO (\square), Y350F TDO (\square), GTGGS-to-GTGGA TDO (\triangle), GTGGS-to-GTGGS TDO (\triangle), and GTGGS-to-GTGGS TDO (\triangle).

References cited

- M. Herger, P. van Roye, D. K. Romney, S. Brinkmann-Chen, A. R. Buller, F. H. Arnold, *J. Am. Chem. Soc.* **2016**, *138*, 8388-8391. I. Barr, F. Guo, *Bio Protoc.* **2015**, *5*, e1594. I. Shin, R. C. Nguyen, S. R. Montoya, A. Liu, *J. Biol. Chem.* **2025**, *301*, 108241. Y. Zhang, Y. Zou, N. L. Brock, T. Huang, Y. Lan, X. Wang, Z. Deng, Y. Tang, S. Lin, *J. Am. Chem. Soc.* **2017**, *139*, 11887-11894. [1] [2]

- [3] [4]

